Mapping the dynamics of epigenetic adaptation

Ajay Larkin[1,5], Colin Kunze[2,3,5], Melissa Seman[1], Alexander Levashkevich[1], Justin Curran[1], Ahmad S. Khalil[2,3,4*], and Kaushik Ragunathan[1*]

[1] Department of Biology, Brandeis University, Waltham, MA 02453

[2]Biological Design Center, Boston University, Boston, MA 02215, USA

[3]Department of Biomedical Engineering, Boston University, Boston, MA 02215, USA

[4]Wyss Institute for Biologically Inspired Engineering, Harvard University, Boston, MA 02115 USA

[5]These authors contributed equally

*Correspondence: kaushikr@brandeis.edu (K.R.), khalil@bu.edu (A.S.K.)

SUMMARY

A classical and well-established mechanism that enables cells to adapt to new and adverse conditions is the acquisition of beneficial genetic mutations. Much less is known about epigenetic mechanisms that allow cells to develop novel and adaptive phenotypes without altering their genetic blueprint. It has been recently proposed that histone modifications, such as heterochromatin-defining H3K9 methylation (H3K9me), normally reserved to maintain genome integrity, can be redistributed across the genome to establish new and potentially adaptive phenotypes. To uncover the dynamics of this process, we developed a precision engineered genetic approach to trigger H3K9me redistribution on-demand in fission yeast. This enabled us to trace genome-scale RNA and chromatin changes over time prior to and during adaptation in long-term continuous cultures. Establishing adaptive H3K9me occurs over remarkably slow time-scales relative to the initiating stress. During this time, we captured dynamic H3K9me redistribution events ultimately leading to cells converging on an optimal adaptive solution. Upon removal of stress, cells relax to new transcriptional and chromatin states rather than revert to their initial (ground) state, establishing a tunable memory for a future adaptive epigenetic response. Collectively, our tools uncover the slow kinetics of epigenetic adaptation that allow cells to search for and heritably encode adaptive solutions, with implications for drug resistance and response to infection.

INTRODUCTION

Adaptation enables cells to survive new or changing environments by establishing novel phenotypes that enhance cell fitness (Brooks et al., 2011; Gasch et al., 2000). These processes are dynamic and constantly reshape how organisms respond to a wide range of physiological contexts that includes how cells in our body respond to infections, cancer cells react to chemotherapeutic agents, and the emerging threat of antibiotic and antifungal resistance amongst microbes (Alberts, 2002; Fisher et al., 2022; Flavahan et al., 2017). One major mechanism that cells leverage to acquire new phenotypes is altering their DNA sequence through genetic mutations (Baker et al., 2018). Although beneficial mutations in populations are rare, cells that acquire such mutations will eventually outcompete those that fail to adapt (Luria and Delbrück, 1943; McKenzie et al., 2000). However, genetic mutations represent an inflexible commitment to a new environment that cannot be reversed following a return to cellular homeostasis (Ravikumar et al., 2018). Furthermore, it is well known that genetic adaptation to one condition is often associated with a fitness loss in other environments and hence such changes may represent sub-optimal and terminal solutions amidst fluctuating environments (Stajic et al., 2022).

An alternative is epigenetic adaptation, whereby cells acquire new phenotypes without any changes to their genetic blueprint (Allis and Jenuwein, 2016). While genetic mutations are irreversible, epigenetic changes can buffer against deleterious mutations without compromising the overall fitness of the cell (Stajic et al., 2022, 2019). In principle, this strategy offers a dynamic, reversible, and flexible form of adaptation well-suited to rapidly changing environmental conditions especially when such conditions persist only for a few generations (Casadesús and Low, 2006; Kussell and Leibler, 2005; Thattai and van Oudenaarden, 2004). Moreover, due to the flexibility of this mode of adaptation, epigenetic changes often pose serious clinical challenges during the evolution of chemotherapy resistance in cancer cells or the widespread emergence of antifungal resistance (Calo et al., 2014; Guler et al., 2017; Liau et al., 2017; Sharma et al., 2010; Torres-Garcia et al., 2020,

2020). Thus, understanding how cells leverage adaptive epigenetic mechanisms and targeting such pathways can help us achieve improved clinical outcomes.

One known example of epigenetic adaptation is prion switching in yeast. In particular, the [*PSI*$^+$] prion is the aggregated, self-propagating form of the yeast translation-termination factor Sup35 (Halfmann et al., 2012; True and Lindquist, 2000). Upon switching to the prion form, the [*PSI*$^+$] prion sequesters soluble (active) Sup35, thereby uncovering previously cryptic genetic variation by promoting genome-wide translation readthrough. Hence, a latent, aggregation-prone, conformational state, when unleashed, can enable cells to acquire novel and heritable phenotypes that may be beneficial in unanticipated conditions. Can other epigenetic pathways be similarly leveraged in an on-demand fashion to unleash latent, heritable, and adaptive phenotypes?

Several lines of evidence suggest that cells have the capacity to alter their transcriptomes in response to stress through stochastic changes in transcription, alterations in chromatin accessibility, rewiring existing regulatory networks, and orchestrating wholesale changes in histone modification states (David et al., 2010; Freddolino et al., 2018; Guler et al., 2017; Kiani et al., 2022; Parmentier et al., 2022; Shaffer et al., 2020, 2017; Tagkopoulos et al., 2008). Moreover, recent work has shown that diverse histone modifications with canonical roles in preserving genome integrity and enforcing cell identity may have adaptive potential by being dynamically redistributed to new genomic loci under different stress conditions (Liau et al., 2017; Sharma et al., 2010; Torres-Garcia et al., 2020). How cells exploit these chromatin-based epigenetic programs to discover genes that can be activated or repressed for enhanced fitness and survival, while ensuring that these adaptive responses are stably inherited across many generations remains mysterious.

To achieve successful adaptation, the dynamic redistribution of histone modifications must in principle meet three critical requirements. The first requirement involves spatial changes in modification states, either through spreading from existing sites or the formation of new islands at novel locations in the genome. This is critical for cells to be able to sample

which genes to silence or activate. The second requirement demands that the resulting histone modification-dependent changes in gene expression benefit cells in their new environment (Raj and van Oudenaarden, 2008). This process ensures that any optimal adaptive solution that cells make is stably maintained within the population. Lastly, the new cell state should be heritable across multiple generations so that cells are prepared to more rapidly respond to a future instance of exposure to the initiating stress (Audergon et al., 2015; Light et al., 2010; Park et al., 2019; Ragunathan et al., 2015; Sump et al., 2022). Thus, to faithfully map epigenetic adaptation pathways, it is necessary to reconstruct these highly dynamic processes and be able to connect genome-wide changes at the RNA and chromatin levels with cell fitness prior to and following adaptation.

To reconstruct these dynamics, we developed an experimental system based on the fission yeast, *Schizosaccharomyces pombe*. In *S. pombe*, H3K9 methylation (H3K9me) specifies silent epigenetic states otherwise referred to as heterochromatin (Allshire and Madhani, 2018). Although heterochromatin normally resides at regulatory regions of the genome, such as centromeres and telomeres, H3K9me can also be deployed to downregulate novel targets (Duempelmann et al., 2019; Halic and Moazed, 2010; Iglesias et al., 2018; Kowalik et al., 2015; Parsa et al., 2018; Pisacane and Halic, 2017; Wei et al., 2021; Yamanaka et al., 2013). One example of an acute stress in *S.pombe* that elicits an adaptive epigenetic response is so-called “heterochromatin misregulation”. Deleting two major H3K9me antagonists – the H3K14 histone acetyltransferase Mst2 and the putative H3K9 demethylase Epe1 – leads to the adaptive silencing of the sole H3K9 methyltransferase, Clr4, suppressing aberrant genome wide H3K9 methylation and restoring fitness (Wang et al., 2015). We reasoned that this system would provide an ideal, minimal, and genetic framework to induce heterochromatin misregulation and unveil the sequence of events that occur prior to adaptation.

Using synthetic biology, we developed a precision genetic approach to trigger and release heterochromatin misregulation on-demand (Basi et al., 1993; Kanke et al., 2011).

Taking inspiration from laboratory evolution experiments, which have been powerful in defining genetic adaptations in microbial populations grown under selective pressure, we coupled this ability to induce heterochromatin misregulation with advanced continuous culture methods that allow us to quantify cell fitness in real-time and identify causal genome-wide transcriptional and chromatin-state changes (Lenski et al., 2015). Our inducible experimental system is a significant departure from previous studies that focused primarily on beginning and end-state measurements or those that depend on small molecule stressors which produce adverse pleiotropic effects on cell physiology (Torres-Garcia et al., 2020, 2020). By quantifying cell-fitness in yeast populations, we could precisely trace the time evolution of the adaptive silencing program under multiple cycles of heterochromatin stress and recovery. Our approach uncovers how cells can redistribute H3K9me, records network-level changes in transcription, and defines how this dynamic interplay unlocks cryptic epigenetic variation to enable cell survival under conditions of acute stress. In summary, our study captures key features of how cells turn an existing regulatory pathway that normally ensures H3K9 methylation is deposited only at constitutive sites into an adaptive mechanism with implications for drug resistance and response to infection.

RESULTS

An inducible Epe1 depletion system to trigger heterochromatin misregulation on-demand

Epe1, a putative H3K9 demethylase, and Mst2, an H3K14 acetyltransferase, have additive roles in regulating *S.pombe* heterochromatin. Deleting both Epe1 and Mst2 leads to acute heterochromatin misregulation, which in turn promotes an adaptive epigenetic response (Wang et al., 2015). We first confirmed previously published results by generating *mst2*Δ *epe1*Δ cells, which successfully adapted by silencing the H3K9 methyltransferase, Clr4. We measured an approximately ~4 fold decrease in Clr4 mRNA levels and the establishment of adaptive H3K9me2 at the *clr4+* locus (**Figure S1A-C**).

Since genetic deletions can only provide an endpoint phenotypic output, we sought to design a system for triggering heterochromatin misregulation on-demand by inducibly, rapidly, and thoroughly depleting Epe1. In principle, such a system would enable us to observe in real-time how cells respond to the induction of acute heterochromatin misregulation and dynamically trace adaptive pathways. We designed a system to control Epe1 protein production at two levels: 1) we replaced the endogenous *epe1+* promoter with a thiamine-repressible promoter (*nmt81*) such that addition of thiamine represses mRNA transcription and 2) we fused an auxin inducible degron tag to the C-terminus of Epe1 to trigger protein degradation. We refer to this inducibly degradable Epe1 allele as $epe1^{deg}$ (**Figure 1A**) (Basi et al., 1993; Kanke et al., 2011). Adding thiamine to cells grown in liquid media caused a rapid 8-fold reduction in Epe1 mRNA levels which, when combined with napthaleneacetic acid (NAA; a synthetic auxin analog), led to the absence of any detectable Epe1 protein in as little as 30 minutes (**Figure 1B-C**). Thus, Epe1 depletion rapidly leads to negligible protein and transcript levels in less than an hour of exposure to NAA and thiamine.

We grew cells overnight and plated equal numbers on non-selective media (white '-' square) or media that contained NAA and thiamine (orange '+' square) and quantified the mean and standard deviation of colony sizes (**Figure 1D**). We observed generally smaller colonies and substantial colony size heterogeneity when we depleted Epe1 in an *mst2*Δ background, reflecting a fitness loss associated with stress (**Figures 1D-E**). Furthermore, *mst2*Δ $epe1^{deg}$ cells exhibited a 4-fold decrease in Clr4 mRNA levels after five days of Epe1 depletion, which recapitulates the adapted state we observed in *mst2*Δ *epe1*Δ cells (**Figure 1F, S1C**). In contrast, depleting Epe1 in an *mst2+* background produced a less pronounced growth defect and no detectable adaptive Clr4 silencing. Hence, despite the absence of Epe1, these cells exhibited no obvious phenotypic change. Furthermore, there was no decrease in Clr4 mRNA for *mst2+* $epe1^{deg}$ cells after five days of Epe1 depletion, consistent with previous studies (Wang et al., 2015).

To test if adaptation was dependent on the order in which the two heterochromatin regulators were depleted, we inverted our genetic background. We developed a strain to deplete Mst2 (*mst2*^{deg}) in an *epe1*Δ background: *mst2*^{deg} *epe1*Δ (**Figure S1D-G**). While there was still some decrease in colony size upon Mst2 depletion, this strain did not produce the same degree of heterogeneity in colony size (**Figure S1D-F**). Additionally, we observed that Clr4 was silenced to a lesser degree compared to *mst2*Δ *epe1*^{deg} cells (**Figure S1G**). This may be because deleting first Epe1 primes cells for adaptation, and suggests a hierarchy between the two heterochromatin regulators, Epe1 and Mst2. Collectively, our results establish a system for the inducible, rapid, and complete depletion of Epe1, and demonstrate that the *epe1*^{deg} allele recapitulates how *S.pombe* cells adapt in response to acute heterochromatin misregulation.

Time evolution of adaptive silencing during heterochromatin misregulation

To trace the time evolution of adaptation following Epe1 depletion, we deployed the automated eVOLVER continuous culture platform (**Figure 2A**) (Heins et al., 2019; Wong et al., 2018). eVOLVER enables long-term maintenance of independent *S.pombe* cultures in miniature bioreactors using a continuous turbidostat routine with real-time growth rate quantification (García-Ruano et al., n.d.; Huang, 2022; Zhong et al., 2020). The eVOLVER system also features the ability to schedule media changes, including switching between non-inducer and inducer media. As a result, we can precisely quantify changes in growth resulting from Epe1 depletion, and sample cells as a function of time for molecular measurements to reconstruct the dynamics of Clr4 silencing and concomitant changes in transcription.

We grew replicate populations of *mst2*Δ *epe1*^{deg} cells in eVOLVER turbidostats for 48 hours at 32°C before switching to inducer (NAA and thiamine-containing) media to trigger Epe1 depletion (Methods). Upon induction, we observed a substantial reduction in growth rate over the course of a 48-hour period (**Figure 2B**). This was followed by a recovery period in which cells returned to pre-depletion growth rates, indicative of adaptation to

heterochromatin misregulation. Based on the eVOLVER time traces, we posited that cells transit through three primary phases upon experiencing heterochromatin misregulation, namely 1) **pre-stress** (before inducing Epe1 depletion) 2) **stress** (post-induction, characterized by poor growth) and, 3) **adapted** (growth recovery). In contrast, no change in growth rate was observed in *mst2*Δ *epe1*^{deg} *clr4*Δ populations upon induction of Epe1 depletion (**Figure S2A**).

To reconstruct time-resolved changes in Clr4 silencing, we harvested cells grown in 24-hour time intervals for quantification of *clr4+* mRNA and H3K9me2/me3 levels. In the initial stress phase (during the first 48 hours post-induction), we observed no changes in *clr4+* mRNA and very minimal increases to H3K9me2/me3 levels (**Figures 2C-E**). However, during the adapted phase (after 48 hours) we observed a substantial decrease in *clr4+* mRNA expression (**Figure 2C**). The change in *clr4+* mRNA levels coincided with enrichment of H3K9me2/3 at the *clr4+* locus, which had remained largely unmarked until that time (**Figure 2C-E**). Thus, the transition between the stress and adapted phases is closely aligned with a steady enrichment of H3K9me2/me3 and reduction in *clr4+* mRNA levels. These results demonstrate that growth rate and Clr4 silencing dynamics are closely coordinated as cells adapt to acute heterochromatin misregulation stress.

To assess transcriptome-wide changes during the time-course of adaptation, we performed RNA-seq on *mst2*Δ *epe1*^{deg} samples that were collected at 24-hour intervals in triplicate. In the stress phase, we observed acute changes to the transcriptome relative to untreated *mst2*Δ *epe1*^{deg} cells (**Figure 2F**). These gene expression changes during the stress phase gradually vanished by the end of the time course such that, by the time adaptation was completed, the transcriptome of Epe1-depleted cells resembled those of pre-stress cells. We applied principal component analysis (PCA) to further investigate the transcriptome changes. PCA clearly captured time-dependent transitions between different growth phases following Epe1 depletion (**Figure 2G, S2B**). Notably, gene expression changes in the stress phase (24-48 hours) and those in the late adapted phase (96-120

hours) cluster into non-overlapping statistically significant groups, with the 72-hour time point falling at the intersection between these two groups.

Adaptation is time-independent in *mst2*Δ *epe1*Δ cells. Hence, we additionally performed RNA-seq analysis on *mst2*Δ *epe1*Δ cells to compare with *mst2*Δ *epe1*^{deg} cells. Most strikingly, the transcriptomes of these cells most closely resembled pre-stress *mst2*Δ *epe1*^{deg} cells (0 hours) (**Figure 2G, S2B**). Importantly, we confirmed that independent *mst2*Δ *epe1*Δ clones have few differences in their transcriptomes, implying that independent isolates also make the same adaptive choices and their gene expression networks are rewired in a very similar manner (**Figure S2C-D**). *mst2*Δ *epe1*Δ cells have silenced *clr4+* and have been grown well beyond 120 hours. Thus, their convergence towards the pre-stress transcriptome implies that there are additional RNA level changes that occur beyond our 120-hour adaptation time-course. For example, we found that, in Epe1-depleted cells at 120 hours, genes associated with iron homeostasis are upregulated while genes associated with ATP synthesis and cellular respiration are downregulated (**Figure S2E-F**), whereas in *mst2*Δ *epe1*Δ cells these genes returned to expression levels equivalent to unstressed *mst2*Δ *epe1*^{deg} cells (**Figure S2G**). Taken together, our system captures, with unprecedented resolution, the time evolution of transcriptome-wide changes that drive epigenetic adaptation revealing distinct population-level cell states during this process.

Heterochromatin misregulation triggers the targeted expansion of pre-existing H3K9me3 islands

To investigate how heterochromatin misregulation drives changes in the H3K9 methylome over time, we cultured *mst2*Δ *epe1*^{deg} cells over six 24-hour periods encompassing the pre-stress, stress, and adapted phases and performed chromatin immunoprecipitation for H3K9me3 followed by deep sequencing (ChIP-seq). We observed expansion of specific H3K9me3 domains, primarily at constitutive heterochromatin (pericentromeres, telomeres, and the ribosomal DNA locus) and several preexisting heterochromatin islands centered around meiotic genes and ncRNAs (**Figure 3A, Figure**

S3A, Table S4) (Yamanaka et al., 2013; Zofall et al., 2012). We observed very little enrichment for H3K9 methylation outside of these core heterochromatin sites. Expansion of H3K9me3 reached a maximum at the end of stress phase (48 hours) followed by a steady decay in the adapted phase at constitutive heterochromatin, non-coding RNAs, and meiotic genes (**Figure 3B-C**). In contrast, H3K9me3 is deposited *de novo* at the *clr4+* locus and accumulates over time (**Figure 3D**). This process is distinct from other H3K9me3 peaks at meiotic genes or ncRNA, which expand during stress and then subsequently retract once cells adapt (**Figure 3E, S3B**).

We cross-referenced our H3K9me3 ChIP-seq and transcriptome time-course data to measure transcriptomic changes caused by aberrant H3K9me spreading during heterochromatin misregulation. We found a total of 753 genes under expanded H3K9me3 peaks during stress phase (48 hours) that were previously not marked by H3K9me3 in the pre-stressed population (**Figure S3C**). Surprisingly, of these 753 genes, a subset of only 113 genes were significantly downregulated (**Figure 3F**). This subset of genes was not functionally enriched for any specific pathways by GO analysis, but notably included a collection of 21 essential genes, including the mitochondrial LYR protein *cup1+* (Torres-Garcia et al., 2020; Yaseen et al., 2022). These essential genes are repressed up until the end of stress phase (48 hours) after which *clr4+* silencing and growth rate recovery coincides with their de-repression (**Figure 3G**). This observation suggests that the downregulation of *cup1+*, and other essential genes proximal to expanding H3K9me3 islands, may correlate with poor cell growth during early heterochromatin misregulation. In contrast, during the adapted phase, there was a dramatic shift in the H3K9me3 methylome. Most genes that were marked by novel H3K9me3 and significantly downregulated were proximal to the *clr4+* locus (**Figure S3D-F**). Together, these results indicate that heterochromatin misregulation drives very targeted expansion of existing H3K9 methylation domains, silencing only a small fraction of essential genes. Additionally, development of facultative heterochromatin over the *clr4+* locus occurs *de novo* and represents a rare

example of a new ectopic site of H3K9 methylation distinct from the targeted expansions of existing sites of H3K9 methylation.

Activation of the cellular stress response pathway is required for survival but not adaptive choice

To identify gene pathways relevant to the stress phase of heterochromatin misregulation, we analyzed the set of differentially expressed genes within the stress phase, envisioning that it is most likely to contain the most critical population-level transcriptomic features required for adaptation. Enriched GO terms in this set included genes involved in ribosome biogenesis, translation, caffeine and rapamycin treatment, nitrogen depletion, and the core environmental stress response (CESR) (**Figure 4A, S4A**) (Chen et al., 2003; Rubio et al., 2021). These results were surprising, given our prior assumption that misregulation of the epigenome is a unique form of stress distinct from other types of environmental stresses. Mapping time-dependent changes across these GO categories reveals that the differential expression of cell proliferation and stress response genes subsides as adaptive Clr4 silencing is established (**Figure 4B, S4B-F**). Considering this apparent relationship, we wanted to interrogate the role that the stress response pathway plays in cell survival during heterochromatin misregulation and adaptive Clr4 silencing.

The CESR pathway plays a major role in *S.pombe* stress response. To interrogate the functional role of CESR during induced heterochromatin misregulation, we deleted the MAP kinase Sty1 in an *mst2*Δ *epe1*^{deg} background. Sty1 regulates stress response in *S.pombe* by phosphorylating transcription factors that activate the expression of stress response genes, including a majority of genes in CESR (**Figure 4C**) (Chen et al., 2003). We plated *mst2*Δ *epe1*^{deg} *sty1*Δ cells on solid media for five days and measured cell colony size and survival frequency (**Figure 4D**). *mst2*Δ *epe1*^{deg} *sty1*Δ colonies were on average smaller than *mst2*Δ *epe1*^{deg} cells, both pre- and post-Epe1 depletion (**Figure 4E**). We observed only half as many colonies formed upon plating *mst2*Δ *epe1*^{deg} *sty1*Δ cells on NAA and thiamine-containing medium compared to *mst2*Δ *epe1*^{deg} cells (**Figure 4F**). However, despite lower

rates of stress-survival, Epe1-depleted *mst2*Δ *epe1*^{deg} *sty1*Δ colonies showed equally strong adaptive silencing of Clr4 transcription compared to *mst2*Δ *epe1*^{deg} (**Figure 4G**). This suggests that the activation of stress response pathways is an on-pathway intermediate prior to adaptation, instead of directly driving redistribution of H3K9 methylation (Ho and Gasch, 2015). Altogether, these results support Sty1 activity as beneficial for survival during heterochromatin misregulation.

Since perturbing stress response pathways did not affect adaptive *clr4+* silencing, we focused on different heterochromatin nucleation factors which could be involved in this selection process. Based on our H3K9me3 ChIP-seq analysis of heterochromatin islands at meiotic genes and ncRNA, we focused on two major heterochromatin nucleation pathways – RNAi (Ago1, Dcr1) and MTREC (Red1) (Egan et al., 2014; Lee et al., 2013; Yamanaka et al., 2013; Zofall et al., 2012). We observed a lesser degree of *clr4+* transcriptional silencing in the adapted phase only in *red1*Δ cells but not *ago1Δ* or *dcr1Δ* cells, suggesting that cells may experience a lesser degree of heterochromatin misregulation stress compared to *red1+* cells (**Figure S4G**) (Wang et al., 2015). To confirm this, we conducted growth experiments using replicate *mst2*Δ *epe1*^{deg} *red1*Δ cultures on plates supplemented with NAA and thiamine, as well as in continuous culture using the eVOLVER system (**Figure S4H-I**). These approaches allowed us to confirm the fitness increase during the stress phase compared to *red1+* cells. Additionally, we compared the results to those obtained from *ago1*Δ and *dcr1*Δ cells, which exhibited the expected loss of fitness. To further quantify and compare loss of fitness during the stress phase, we calculated the mean minimum decrease in growth rates for each eVOLVER experiment (**Methods**). Red1-deficient cultures displayed a significantly smaller decrease in growth rate, similar to *mst2*Δ *epe1*^{deg} *clr4*Δ, compared to *mst2*Δ *epe1*^{deg} or RNAi deletions (**Figure S4J**). Hence, these results suggest that MTREC mediated Clr4 recruitment may nucleate aberrant heterochromatin during the stress phase (Dobrev et al., 2021; Foucher et al., 2022; Soni et al., 2023).

Adaptive heterochromatin exhibits memory upon re-induction of stress

As we previously showed, depletion of Epe1 is rapid and efficient, occurring in as little as 30 minutes after the addition of NAA and thiamine (**Figure 1C**). Therefore, the *epe1*^{deg} allele enables us to rapidly and reversibly cycle between Epe1 depletion and expression. To test whether cells that had adapted to Epe1 loss also exhibited memory, we restored Epe1 expression in adapted cells for different recovery periods. We refer to these recovery periods as **short** (24 hours), **medium** (48 hours) and **long** (72 hours). Following the recovery period, we re-initiated Epe1 depletion to generate a second stress phase (**Figure 5A, S5A**). If the adaptive response (as measured by Clr4 silencing) is faster during the second stress phase, it would imply that cells have memory.

As controls, pre-stress cells exhibited smaller sized colonies with substantial heterogeneity upon Epe1 depletion (**Figure 5B**). Adapted cells exhibited uniformly sized colonies upon sustained Epe1 depletion. In contrast, adapted cells that had experienced a short recovery dose of Epe1 (Epe1 re-expressed for 24 hours) produced an intermediate colony size phenotype, with a bimodal distribution of small and large colonies. These results suggest that some proportion of short recovery cells had reverted to the pre-stress state while others preserved the adapted state during the 2nd stress phase. Medium and long recovery cell populations produced colony size phenotypes that matched pre-stress cells, suggesting that a prolonged recovery phase (>24 hours) led to the complete loss of adaptive memory. Hence, our results reveal that a memory associated with heterochromatin misregulation can persist for about 24 hours (~6-8 cell generations) following the removal of the initiating stress.

We observed that *clr4+* expression recovered to pre-stress levels during the short recovery period and this was associated with a complete loss of adaptive H3K9me3 (**Figure 5C-D, S5B**). Nevertheless, short recovery cells exhibited faster re-silencing of Clr4, which was associated with the re-establishment of H3K9me3 on timescales that surpassed pre-stress cells (24 hours in short recovery cells versus 72 hours in naive cells). Our results implied that the memory associated with Clr4 re-silencing did not depend on H3K9me3 being

retained during the short recovery period. Therefore, we tested whether short recovery cells exhibited other transcriptional changes that could account for prolonged adaptive memory. We performed RNAseq analysis on short and medium recovery cell populations. Indeed, PCA reveals that cells during recovery phases exhibit unique transcriptional dynamics that were distinct from pre-stress, stress, or adapted phase cells (**Figure 5E, S5C**). Importantly, the cell transcriptional state when Epe1 is re-expressed does not instantaneously revert to the initial pre-stress state. Transcriptional changes in the short recovery phase were primarily enriched for genes related to ncRNA and rRNA processing, ribosome biogenesis, and RNA metabolic processes (**Figure S5D**). We also observed enrichment for CESR transcripts, suggesting that the shift from the adapted state and loss of heterochromatin at *clr4+* activates part of a stress response. Since we have previously implicated MTREC in adaptive Clr4 silencing, we examined known Red1 targets (**Figure S4G-I, S5E**) (Bitton et al., 2015; Hasan et al., 2014). We observed large transcriptional changes in Red1 targets during both the stress and recovery phase, reinforcing the causal role that MTREC has in adaptive Clr4 silencing. Collectively, these observations highlight several network level changes, in addition to H3K9me3 regulation, that could contribute towards adaptive memory.

The time scale of adaptive memory can be tuned by histone acetylation

Cells may need to extend or even erase memory associated with past events (Light et al., 2010; Sump et al., 2022). To identify chromatin-based mechanisms that might modulate and even enhance adaptive memory duration, we considered the interdependence of H3K9me with other histone modifications. Histone hyperacetylation (H3K9Ac, H3K14Ac, H3K18Ac) and histone turnover are characteristic features of actively transcribed genes, and loss of histone acetylation can promote heterochromatin inheritance (Aygün et al., 2013; Johnsson et al., 2009). Although Mst2 has been deleted in these strains, it is possible that other histone acetyltransferases could play additive roles in tuning adaptive memory (Zofall et al., 2022). We deleted a second acetyltransferase, Gcn5 in a *mst2*Δ *epe1*^{deg} background (*mst2*Δ *gcn5*Δ *epe1*^{deg}). We performed memory experiments as previously described where

we now cycled *mst2*Δ *gcn5*Δ *epe1*^{deg} cells between conditions where Epe1 was depleted or expressed. Unlike what we observed in cells where Gcn5 is present (memory decayed after the short recovery period), *mst2*Δ *gcn5*Δ *epe1*^{deg} cells retained memory after short, medium, and long recovery periods. After each recovery period, colony sizes most closely resembled adapted colonies, implying that these cells may exhibit prolonged, adaptive memory (**Figure 6A**).

Next, we measured other molecular correlates of memory, which includes *clr4+* mRNA levels and H3K9me3 levels at the *clr4+* locus using ChIP qPCR. We made two important observations: **1)** First, during each recovery phase, *clr4+* mRNA levels reverted to high levels of transcription, matching what we typically observed in pre-stress cells. Yet, in every instance, cells retained residual levels of H3K9me3 at the *clr4+* locus (**Figure 6B**). Although residual H3K9me3 levels were still present, they did not appear to have a repressive function during the recovery phase. **2)** Second**,** when exposed to a 2nd stress, *gcn5Δ* cells silenced *clr4+* and established adaptive H3K9me3 on much faster timescales than in the case of *gcn5+* cells (**Figure 6B-D**). Hence, altering the chromatin state and the persistence of H3K9me3 at the *clr4+* locus has an additive effect on adaptive memory. The interdependence on multiple chromatin modifications may allow for cells to rapidly toggle adaptive silencing states enabling them to extend (or erase) memory of past stress events.

DISCUSSION

Cells can repurpose and leverage existing epigenetic pathways to modulate gene expression states in response to environmental change. In fission yeast, H3K9 methylation exhibits adaptive epigenetic potential that is unlocked when cells encounter various environmental stressors, including anti-fungals, caffeine, or nutrient restriction (Bao et al., 2022; Hirai et al., 2022; Torres-Garcia et al., 2020; Yaseen et al., 2022). These stressors affect the levels of two major H3K9me regulators, Epe1 and Mst2 (Torres-Garcia et al., 2020). Therefore, our ability to control Epe1 levels rapidly and reversibly enables us to mimic the natural response of fission yeast cells to stress, independent of an initiating stress. Our

system enables the capture of early and intermediate transcriptional states that lead to adaptive silencing of *clr4+*, observations that would be impossible using conventional genetic methods.

Notably and surprisingly, we found that the decision for cells to adapt and silence *clr4+* is a slow process, taking up to 120 hours, which is two orders of magnitude slower than the timescale of Epe1 depletion (approximately 30 minutes). We propose that these slow dynamics may represent a bet-hedging strategy, where cells reversibly sample different transcriptional states to enhance fitness before converging on an optimal solution (Ogura et al., 2016). Our findings parallel stochastic tuning models in budding yeast, which posit that transcriptional noise is positively selected to promote cell survival in novel environmental conditions (David et al., 2010; Freddolino et al., 2018).

By analyzing the transcriptomic profile of cells, we observed transient activation of stress response pathways correlating with a slow growth phenotype. Activation of genes associated with the core environmental stress response (CESR) serve as an on-pathway intermediate preceding adaptation (Ho and Gasch, 2015). These dynamics strikingly resemble how cancer cells often vexingly develop resistance, resulting in poor prognosis and treatment outcomes. For example, glioblastoma cells transiently exit the cell cycle, exhibit slow growth, misregulate H3K27 methylation-dependent epigenetic pathways, and ultimately adapt by entering a state that is refractory to chemotherapeutic interventions (Liau et al., 2017). Bacteria also enter slow-growing persister states through the activation of a stress-induced SOS pathway, leading to genetic changes and antibiotic resistance (Cairns et al., 1988; McKenzie et al., 2000). In both instances, slow growth is a common denominator that is triggered by the activation of the stress response pathway. Thus, the activation of stress response pathways may represent a general principle that cells leverage to explore adaptive phenotypes when exposed to novel environments (Ho and Gasch, 2015).

It is possible that the initial, unregulated expansion of H3K9me during early heterochromatin misregulation leads to the silencing of many essential genes that disrupt

fitness and cell survival. We speculate that this could represent a temporary switch in growth strategy to a slow proliferation state until beneficial adaptations can be acquired. The expansion of heterochromatin domains over essential genes could also act as a filter for stress and adaptive responses. Since the spatial expansion of heterochromatin must build over time, cells would need to experience sustained exposure to a stressor before committing to adaptive H3K9me redistribution, preventing premature adaptive responses to transient environmental perturbations.

Establishing adaptive heterochromatin at the *clr4+* locus follows unique dynamics that are distinct from H3K9me-spreading at other regions during heterochromatin misregulation. These dynamics suggest active recruitment of heterochromatin initiation and maintenance factors that have adaptive potential. This process is partially dependent on Red1, as *mst2*Δ *epe1*^{deg} *red1*Δ cells consistently show weaker *clr4+* adaptive silencing within our 120-hour window, and an increase in fitness during the stress phase. This raises the possibility that adaptive silencing is mediated by co-transcriptional or post-transcriptional processes that involve non-coding RNA recognition by factors that are part of the MTREC complex (Egan et al., 2014; Lee et al., 2013; Zofall et al., 2012). The expansion of Red1-dependent H3K9me islands during the stress phase may have a causal role in activating stress response pathways, thus explaining why deleting Red1 alleviates heterochromatin misregulation. Alternatively, Red1 may be involved in nucleating H3K9me islands *de novo* at potential targets for silencing which may have adaptive potential. How this RNA elimination machinery might affect the formation of *de novo* adaptive heterochromatin in other stress contexts, and the extent to which it can be repurposed when cells encounter novel environments, requires further investigation.

Our unique ability to toggle between Epe1 removal and expression enabled us to determine that cells can retain a memory associated with prior heterochromatin misregulation for approximately 6-8 generations following the initial stress. This memory persists, despite H3K9me being completely erased from the *clr4+* locus upon Epe1

reintroduction. Because memory can persist without any detectable levels of H3K9me at the *clr4+* locus (although residual H3K9 methylation cannot be ruled out), we speculated that the origins of memory rely on the cell being poised to adapt due to novel network-level gene expression changes (Holoch et al., 2021; Huang, 2022; Parmentier et al., 2022). Our RNA-seq measurements and PCA analysis firmly support the idea of new adaptive cell states that can encode memory. Cells in which Epe1 has been reintroduced during the recovery phase exhibit unique gene expression signatures, distinct from the pre-stress state. We propose that this feature represents a form of cellular hysteresis, or history dependence, in which case the gene regulatory network in cells is completely rewired upon either removing or adding back Epe1 (**Figure 6E**) (Kramer and Fussenegger, 2005). It remains to be seen whether other epigenetic regulators also exhibit hysteresis given the slow kinetics of establishing novel epigenetic states and histone turnover (Tatarakis et al., 2023).

A major question in our understanding of how cells establish and maintain epigenetic states is whether memory resides within interconnected expression patterns that specify individual cell states or cis-regulatory chromatin-associated changes (Holoch et al., 2021; Huang, 2022; Parmentier et al., 2022). One mode of regulation involves *cis* regulatory changes that preserve memory locally while a second mode involves a gene regulatory network that is wired to reinforce *cis* acting chromatin changes that promote adaptation. One canonical example of *cis* regulation is how high levels of sequence-specific transcription factors- Oct4, Sox2, Klf4, and c-myc -can drive differentiated cells to an induced pluripotent state and influence cellular differentiation (Takahashi and Yamanaka, 2006). Moreover, the epigenetic properties of cells can alter the efficiency of cell state transitions, highlighting the interpretive and additive role of chromatin modifications in transducing cis-regulatory changes (Chen et al., 2013; Holoch et al., 2021). Cycling Epe1 availability reveals that *clr4+* silencing can be established more rapidly following initial exposure to heterochromatin misregulation, independent of pre-existing H3K9 methylation. Additionally, the extent of

memory can be tuned by modifying histone acetylation, which extends the durability of H3K9 methylation during recovery.

In conclusion, our inducible system uniquely allowed us to capture the highly dynamic and unexpected changes in gene expression and chromatin state following acute heterochromatin misregulation in yeast populations, changes that would be otherwise obscured in conventional genetic assays. Using this approach, we could faithfully reconstruct the pathways that cells undertake prior to and during adaptation as well as investigate how the adapted state is memorized across multiple generations**.** Our findings reveal a number of key and distinguishing features of adaptation by epigenetic responses, including the slow kinetics of the process consistent with the concept of epigenetic bet-hedging, and the establishment of adaptive memory that is influenced by cellular history.

METHODS

Yeast strains, plasmid construction, and culturing

All *S. pombe* yeast strains used in this study were generated using either established methods for lithium acetate or electroporation transformations, or by meiotic crossing followed by tetrad dissection. All strains were genotyped using a colony PCR protocol. Plasmid constructs to create modified nmt81-Epe1-3xFlag-AID and nmt81-Mst2-3xFlag-AID inserts were constructed by modifying an existing pFA6a 3xflag AID IAA-17 degron kanMX6 plasmid. Full plasmids were made using ligation methods following PacI digestion to insert the nmt81 promoter. This insert repaired the PacI site, allowing for a second PacI digestion to insert the CDS for Epe1 or Mst2.

EMMC was used as the base media for all cell culturing experiments, and all cultures were grown at 32C. For experiments involving sampling cultures over a time-course, a small volume of cells from each timepoint culture was used to nucleate the culture for the next timepoint in the appropriate media. All strains used in this study are listed in Table 1.

For colony size quantification, seed cultures were grown overnight at 32C in EMMC in liquid media. Seed cultures were then used to nucleate fresh liquid cultures at a low starting OD (< 0.3 OD) and allowed to grow for about 6-8 hours. An equivalent number of cells were then diluted and plated on solid media, either EMMC or EMMC media supplemented with 15mM thiamine and 500mM NAA, and spread with sterile glass beads. Plated cultures were grown at 32C, and pictures were taken at 3 and 5 days from plating on a Biorad ChemiDoc with white epifluorescence. Images were analyzed in FIJI for trimming plate edges, identifying individual cell colonies, and quantifying colony number and size. To calculate percentage survival, we calculated colony count ratios between EMMC and EMMC media supplemented with 15mM thiamine and 500mM NAA.

Western blotting

To test time-dependent depletion of Epe1, cultures were seeded at a low OD (~0.3) in liquid media EMMC or EMMC supplemented with 15mM thiamine and 500mM NAA. For later memory experiments that switched Epe1 expression, cells cultured for five days in 15mM thiamine and 500mM NAA were harvested and a portion of the culture was used to start a new overnight culture in EMMC. This EMMC culture was then both harvested after 24 hours and used to inoculate a new culture in 15mM thiamine and 500mM NAA for a second time. That culture was then sampled after an additions 24 hours. All cultures were harvested by centrifuging 3-5 OD, decanting supernatant, and storing harvested pellets at -80C.

To extract protein for immunoblotting, cell pellets were processed using a standard TCA precipitation protocol. Pellets were washed with 1mL of ice cold water, then resuspended in 150uL of YEX buffer (1.85 M NaOH, 7.5% beta-mercaptoethanol). Resuspended pelleted were incubated on ice for ten minutes, then 150uL of 50% TCA was mixed into each sample and incubated for ten minutes on ice. Samples were then centrifuged for 5 minutes at 13000 rpm at 4C, after which the supernatant was decanted. Pellets were then resuspended in SDS sample buffer (125mM TRB pH 6.8, 8M urea, 5% SDS, 20% glycerol, 5% BME) and centrifuged for 5 minutes at 13000 rpm at 4C. Samples were then run on an SDS page gel at

45 minutes at 200V. Stain-free imaging was performed on a Biorad ChemiDoc. Gel transfer was then performed on a Trans-Blot Turbo Transfer to a nitrocellulose membrane. Immunoblotting was performed by blocking the nitrocellulose membrane with 5% non-fat dry milk in Tris-buffered saline pH 7.5 with 0.1% Tween-20 (TBST) for about an hour. Blots were then incubated overnight with primary antibody at 4C, then washed with TBST three times and incubated with secondary antibody for an hour. Incubated blots were imaged using enhanced chemiluminescence on a Biorad ChemiDoc.

eVOLVER growth assay

Continuous culture experiments were performed in eVOLVER, designed and set up as previously described (Wong et al., 2018). Two replicate cultures of each strain were grown in 25 mL of EMMC media at 32 C. Growth was maintained in log phase using “turbidostat” mode to constrain optical density between 0.1 and 0.6. When cultures rise beyond the maximum OD, a dilution event is triggered, and growth rate is calculated for the duration since the previous dilution by fitting OD measurements to the exponential equation: $OD600 = (initial\ density) * e^{(growth\ rate) * (time)}$. Media condition changes were executed by spiking individual culture vials as well as the input EMMC media with a 1000x concentrated solution of thiamine + NAA in DMSO. Influx and efflux operations were manually triggered to flush untreated media from the lines.

To calculate the time derivative decrease in growth rate post-Epe1 depletion, first 60 hrs (2.5 days) after addition of thiamine and NAA were considered. Time derivatives of growth rate were calculated at each pair of consecutive growth rates with MATLAB's gradient function. A moving average with a sliding window of length 3 was applied to the time derivative of the growth rate, and the minimum of this moving average was found to be the minimum change in growth rate for each experiment vial. Subsequently, the average and standard deviation of the minimum change in growth rate was calculated across triplicate experiment vials.

qRT-PCR and RNA sequencing analysis

Cultures were grown in liquid culture containing either EMMC media or EMMC media supplemented with 15mM thiamine and 500mM NAA. Cells were growth to 0.3-1.0 OD and harvested by centrifuging ~10mL of culture at 2000 rpm for 2 minutes. Cell pellets were washed once in distilled water, centrifuged at 5000 rpm for 30 seconds, and stored at -80C.

Stored pellets were thawed on ice for 5 minutes, then resuspended in 750uL TES buffer (0.01M Tris pH7.5, 0.01M EDTA, 0.5% SDS). 750uL acidic phenol chloroform was immediately added afterwards, samples were vortexed, and then incubated on a heat block at 65C. Samples were incubated for a total of 40 minutes, with 20 seconds of vortexing every 10 minutes. Afterwards, heated samples were placed on ice for 1 minute, shaken, and transferred to phase lock tubes. Phase lock tubes were centrifuged for 5 minutes at 13,000 rpm at 4C, and the aqueous phase was transferred to a clean Eppendorf tube and ethanol precipitated. Isolated nucleic acids were then treated with DNAse I at 37C for 10 minutes and cleaned up on Qiagen RNeasy Clean-Up columns. Purified total RNA was converted to cDNA by annealing reverse primers complementary to target genes and reverse transcribing with SuperScript III Reverse Transcriptase (Invitrogen). qRT-PCR was performed with SYBR Green dye on a CFX Opus 384 Real-Time PCR System. All qRT experiments were reproduced for at least three independently growth replicates.

Libraries were prepared and sequencing was performed commercially. Raw fastq files were evaluated using FastQC (v0.11.9) and trimmed using Trimmomatic (v0.39) and aligned to the ASM294v2 *S. pombe* reference genome using STAR (v2.7.8a) then indexed using samtools (v1.10) (Andrews, 2010; Bolger et al., 2014;Dobin et al., 2013; Danecek et al., 2021). Bam files were grouped by genotype replicate and differential expression analysis was performed through Defined Region Differential Seq in the open source USEQ program suite (v9.2.9) (http://useq.sourceforge.net;Love et al., 2014). The cutoff for significant differential expression of pairwise gene comparisons was defined as a P value of <0.01 (prior to phred transformation) after Benjamini and Hochberg multiple testing corrections. For principal component analysis, rlog counts were used to perform MDS analysis, and custom

ggplot2 R scripts were used to generate scatterplot figures. Volcano plots were drawn using the ggplot2 library, and heatmaps were drawn using the pheatmap library, as well as the standard R library and functions. Gene Ontology analysis was performed using the web-based tool AnGeLi with a p-value cutoff of < 0.01 with FDR correction for multiple testing and default settings (Britton et al., 2015). Raw and processed data are deposited in GEO under the accession number GSE235808.

Chromatin immunoprecipitation, ChIP-seq library preparation and analysis

Cultures were grown in liquid culture containing either EMMC media or EMMC media supplemented with 15mM thiamine and 500mM NAA. Cells were growth to mid-log phase (0.9-1.6 OD) and then harvested by fixation with 1% formaldehyde for 15 minutes then quenched with glycine for 5 minutes. Fixed cultures were then centrifugated, washed twice with 1xTBS, and stored at -80C. To process samples, frozen pellets were thawed at RT for 5 minutes, then resuspended in 300 uL chip lysis buffer (50 mM HEPES-KOH, pH 7.5, 100 mM NaCl, 1 mM EDTA, 1% Triton X-100, 0.1% SDS, and protease inhibitors). Glass beads (500uL, 0.5mm) were added to each tube and cells were lysed by beat beating in an Omni Bead Ruptor at 3000 rpm × 30 s × 10 cycles. Ruptured cells were then collected by using a heated sterile needle to pierce the bottom of each tube, then collecting the lysate in a fresh tube via centrifugation. Lysate was then sonicated in a Q800R3 Sonicator to fragment sizes ranging from 100-500 base pairs. Sonicated lysate was then centrifuged at 13,000 rpm for 15 minutes at 4C, and the liquid portion was transferred to a new tube. Protein content was normalized using a Bradford assay. 25uL of each sample was reserved as input, to which 225uL 1xTE/1%SDS was added. Protein A Magnetic Dynabeads were preincubated with either Anti-H3K9me2 [Abcam, ab1220] or Anti-H3K9me3 [Active Motif, 39161] antibody. 30uL beads preincubated with 2ug antibody was added to 500uL cell lysate and incubated for 3 hours at 4C. Beads were held on a magnetic stand for subsequent washing cycles. For each wash cycle, cells were centrifuged at 1000 rpm for 1 minute at 4C, placed on the magnetic stand and allowed to settle, then liquid was removed by vacuum pipette. Then 1mL

wash buffer was added and samples were rotated for 5 minutes per wash. Samples were washed three times with chip lysis buffer, then once with 1xTE. Samples were then eluted by suspending the beads in 100uL 1xTE/1%SDS for 5 minutes at 65C, then extracting liquid. A second elution was performed with 150uL 1xTE/0.67%SDS. Input and immunoprecipitated samples were then incubated overnight at 65C. We then added 60ug glycogen, 100ug proteinase K, 44uL of 5M LiCl, and 250uL of 1xTE was added to each sample and incubated at 55C for 1 hour. DNA was then extracted using phenol chloroform extraction, followed by ethanol precipitation. Ethanol precipitated pellets were resuspended in 100uL 10mM Tris pH 7.5 and 50mM NaCl. qPCR was performed with SYBR Green dye on a CFX Opus 384 Real-Time PCR System. All ChIP experiments were reproduced for at least two independently grown replicates.

Libraries were prepared following the standard protocol for the NEBNext Ultra II DNA Library Prep kit and sequenced on an Illumina Nextseq instrument. Raw fastq reads were evaluated using FastQC (v0.11.9) and trimmed using Trimmomatic (v0.39) (Andrews, 2010; Bolger et al., 2014). Trimmed reads were aligned to the ASM294v2 *S.pombe* reference genome using the Burrows-Wheeler Aligner (v0.7.17) and bam files were further processed using samtools (v1.10) (Li and Durbin, 2010; Danecek et al. 2021). Bedgraph coverage files were generated using deepTools (v3.5.1) and normalized IP against input in SES mode (Ramírez et al., 2016; Diaz et al., 2012). ChIP-seq H3K9me3 peaks were called using MACS2 with -g 12.57e6 in broad mode with a cutoff of 0.05 (Zhang et al., 2008). Bedtools intersect (v2.27.1) was used to identify genes overlapping with identified peaks. Heatmaps were generated using deepTools (v3.5.1) (Ramírez et al., 2016). Specific peak histograms were generated using the SushiR package and custom R scripts. Two ChIP-seq replicates were produced and processed similarly and showed identical enrichment post-analysis. Raw and processed data are deposited in GEO under the accession number GSE235808.

ACKNOWLEDGMENTS

The authors declare no competing interests. We thank Danesh Moazed for sharing fission yeast strains used in this study. We thank Nidhi Khurana and Gulzhan Raiymbek for their support in obtaining preliminary data during the initial phase of this study. We thank Peter Freddolino, Basila Moochickal Assainar, and Sumanth Maheshwaram for their supportive and insightful feedback regarding this study. We thank Tommy V. Vo for helping with ChIP-seq analysis. This work was supported by the National Science Foundation (NSF) (grant no. EF-1921677 to K.R. and A.S.K.), National Institutes of Health (NIH) (grant nos. R35GM137832 to K.R.; R01EB029483, R01EB027793, and R01AI171100 to A.S.K.); T32GM007544 to A.L.; T32GM007315 to M.S.), Department of Defense Vannevar Bush Faculty Fellowship (no. N00014-20-1-2825 to A.S.K.), and Schmidt Science Polymath Award (no. G-22-63292 to A.S.K.).

REFERENCES

Alberts, B. (Ed.), 2002. Molecular biology of the cell, 4th ed. ed. Garland Science, New York.

Allis, C.D., Jenuwein, T., 2016. The molecular hallmarks of epigenetic control. Nat Rev Genet 17, 487–500. https://doi.org/10.1038/nrg.2016.59

Allshire, R.C., Madhani, H.D., 2018. Ten principles of heterochromatin formation and function. Nat Rev Mol Cell Biol 19, 229–244. https://doi.org/10.1038/nrm.2017.119

Audergon, P.N.C.B., Catania, S., Kagansky, A., Tong, P., Shukla, M., Pidoux, A.L., Allshire, R.C., 2015. Restricted epigenetic inheritance of H3K9 methylation. Science 348, 132–135. https://doi.org/10.1126/science.1260638

Aygün, O., Mehta, S., Grewal, S.I.S., 2013. HDAC-mediated suppression of histone turnover promotes epigenetic stability of heterochromatin. Nat Struct Mol Biol 20, 547–554. https://doi.org/10.1038/nsmb.2565

Baker, S., Thomson, N., Weill, F.-X., Holt, K.E., 2018. Genomic insights into the emergence and spread of antimicrobial-resistant bacterial pathogens. Science 360, 733–738. https://doi.org/10.1126/science.aar3777

Bao, K., Shan, C.-M., Chen, X., Raiymbek, G., Monroe, J.G., Fang, Y., Toda, T., Koutmou, K.S., Ragunathan, K., Lu, C., Berchowitz, L.E., Jia, S., 2022. The cAMP signaling pathway regulates Epe1 protein levels and heterochromatin assembly. PLoS Genet 18, e1010049. https://doi.org/10.1371/journal.pgen.1010049

Basi, G., Schmid, E., Maundrell, K., 1993. TATA box mutations in the Schizosaccharomyces pombe nmt1 promoter affect transcription efficiency but not the transcription start point or thiamine repressibility. Gene 123, 131–136. https://doi.org/10.1016/0378-1119(93)90552-E

Bitton, D.A., Schubert, F., Dey, S., Okoniewski, M., Smith, G.C., Khadayate, S., Pancaldi, V., Wood, V., Bähler, J., 2015. AnGeLi: A Tool for the Analysis of Gene Lists from Fission Yeast. Front. Genet. 6. https://doi.org/10.3389/fgene.2015.00330

Brooks, A.N., Turkarslan, S., Beer, K.D., Yin Lo, F., Baliga, N.S., 2011. Adaptation of cells to new environments. WIREs Mechanisms of Disease 3, 544–561. https://doi.org/10.1002/wsbm.136

Cairns, J., Overbaugh, J., Miller, S., 1988. The origin of mutants. Nature 335, 142–145. https://doi.org/10.1038/335142a0
Calo, S., Shertz-Wall, C., Lee, S.C., Bastidas, R.J., Nicolás, F.E., Granek, J.A., Mieczkowski, P., Torres-Martínez, S., Ruiz-Vázquez, R.M., Cardenas, M.E., Heitman, J., 2014. Antifungal drug resistance evoked via RNAi-dependent epimutations. Nature 513, 555–558. https://doi.org/10.1038/nature13575
Casadesús, J., Low, D., 2006. Epigenetic Gene Regulation in the Bacterial World. Microbiol Mol Biol Rev 70, 830–856. https://doi.org/10.1128/MMBR.00016-06
Chen, D., Toone, W.M., Mata, J., Lyne, R., Burns, G., Kivinen, K., Brazma, A., Jones, N., Bähler, J., 2003. Global Transcriptional Responses of Fission Yeast to Environmental Stress. MBoC 14, 214–229. https://doi.org/10.1091/mbc.e02-08-0499
Chen, Jiekai, Liu, H., Liu, J., Qi, J., Wei, B., Yang, J., Liang, H., Chen, Y., Chen, Jing, Wu, Y., Guo, L., Zhu, J., Zhao, X., Peng, T., Zhang, Y., Chen, S., Li, X., Li, D., Wang, T., Pei, D., 2013. H3K9 methylation is a barrier during somatic cell reprogramming into iPSCs. Nat Genet 45, 34–42. https://doi.org/10.1038/ng.2491
David, L., Stolovicki, E., Haziz, E., Braun, E., 2010. Inherited adaptation of genome-rewired cells in response to a challenging environment. HFSP Journal 4, 131–141. https://doi.org/10.2976/1.3353782
Dobrev, N., Ahmed, Y.L., Sivadas, A., Soni, K., Fischer, T., Sinning, I., 2021. The zinc-finger protein Red1 orchestrates MTREC submodules and binds the Mtl1 helicase arch domain. Nat Commun 12, 3456. https://doi.org/10.1038/s41467-021-23565-3
Duempelmann, L., Mohn, F., Shimada, Y., Oberti, D., Andriollo, A., Lochs, S., Bühler, M., 2019. Inheritance of a Phenotypically Neutral Epimutation Evokes Gene Silencing in Later Generations. Molecular Cell 74, 534-541.e4. https://doi.org/10.1016/j.molcel.2019.02.009
Egan, E.D., Braun, C.R., Gygi, S.P., Moazed, D., 2014. Post-transcriptional regulation of meiotic genes by a nuclear RNA silencing complex. RNA 20, 867–881. https://doi.org/10.1261/rna.044479.114
Fisher, M.C., Alastruey-Izquierdo, A., Berman, J., Bicanic, T., Bignell, E.M., Bowyer, P., Bromley, M., Brüggemann, R., Garber, G., Cornely, O.A., Gurr, Sarah.J., Harrison, T.S., Kuijper, E., Rhodes, J., Sheppard, D.C., Warris, A., White, P.L., Xu, J., Zwaan, B., Verweij, P.E., 2022. Tackling the emerging threat of antifungal resistance to human health. Nat Rev Microbiol 20, 557–571. https://doi.org/10.1038/s41579-022-00720-1
Flavahan, W.A., Gaskell, E., Bernstein, B.E., 2017. Epigenetic plasticity and the hallmarks of cancer. Science 357, eaal2380. https://doi.org/10.1126/science.aal2380
Foucher, A.-E., Touat-Todeschini, L., Juarez-Martinez, A.B., Rakitch, A., Laroussi, H., Karczewski, C., Acajjaoui, S., Soler-López, M., Cusack, S., Mackereth, C.D., Verdel, A., Kadlec, J., 2022. Structural analysis of Red1 as a conserved scaffold of the RNA-targeting MTREC/PAXT complex. Nat Commun 13, 4969. https://doi.org/10.1038/s41467-022-32542-3
Freddolino, P.L., Yang, J., Momen-Roknabadi, A., Tavazoie, S., 2018. Stochastic tuning of gene expression enables cellular adaptation in the absence of pre-existing regulatory circuitry. eLife 7, e31867. https://doi.org/10.7554/eLife.31867
García-Ruano, D., Jain, A., Heins, Z.J., Wong, B.G., Wolle, Y., Khalil, A.S., Coudreuse, D., n.d. Long-term evolution of proliferating yeast cells using the eVOLVER platform.
Gasch, A.P., Spellman, P.T., Kao, C.M., Carmel-Harel, O., Eisen, M.B., Storz, G., Botstein, D., Brown, P.O., 2000. Genomic Expression Programs in the Response of Yeast Cells to Environmental Changes. MBoC 11, 4241–4257. https://doi.org/10.1091/mbc.11.12.4241
Guler, G.D., Tindell, C.A., Pitti, R., Wilson, C., Nichols, K., KaiWai Cheung, T., Kim, H.-J., Wongchenko, M., Yan, Y., Haley, B., Cuellar, T., Webster, J., Alag, N., Hegde, G., Jackson, E., Nance, T.L., Giresi, P.G., Chen, K.-B., Liu, J., Jhunjhunwala, S., Settleman, J., Stephan, J.-P., Arnott, D., Classon, M., 2017. Repression of Stress-

Induced LINE-1 Expression Protects Cancer Cell Subpopulations from Lethal Drug Exposure. Cancer Cell 32, 221-237.e13. https://doi.org/10.1016/j.ccell.2017.07.002
Halfmann, R., Jarosz, D.F., Jones, S.K., Chang, A., Lancaster, A.K., Lindquist, S., 2012. Prions are a common mechanism for phenotypic inheritance in wild yeasts. Nature 482, 363–368. https://doi.org/10.1038/nature10875
Halic, M., Moazed, D., 2010. Dicer-Independent Primal RNAs Trigger RNAi and Heterochromatin Formation. Cell 140, 504–516. https://doi.org/10.1016/j.cell.2010.01.019
Hasan, A., Cotobal, C., Duncan, C.D.S., Mata, J., 2014. Systematic Analysis of the Role of RNA-Binding Proteins in the Regulation of RNA Stability. PLoS Genet 10, e1004684. https://doi.org/10.1371/journal.pgen.1004684
Heins, Z.J., Mancuso, C.P., Kiriakov, S., Wong, B.G., Bashor, C.J., Khalil, A.S., 2019. Designing Automated, High-throughput, Continuous Cell Growth Experiments Using eVOLVER. JoVE 59652. https://doi.org/10.3791/59652
Hirai, H., Takemata, N., Tamura, M., Ohta, K., 2022. Facultative heterochromatin formation in rDNA is essential for cell survival during nutritional starvation. Nucleic Acids Research 50, 3727–3744. https://doi.org/10.1093/nar/gkac175
Ho, Y.-H., Gasch, A.P., 2015. Exploiting the yeast stress-activated signaling network to inform on stress biology and disease signaling. Curr Genet 61, 503–511. https://doi.org/10.1007/s00294-015-0491-0
Holoch, D., Wassef, M., Lövkvist, C., Zielinski, D., Aflaki, S., Lombard, B., Héry, T., Loew, D., Howard, M., Margueron, R., 2021. A cis-acting mechanism mediates transcriptional memory at Polycomb target genes in mammals. Nat Genet 53, 1686–1697. https://doi.org/10.1038/s41588-021-00964-2
Huang, S., 2022. Towards a unification of the 2 meanings of “epigenetics.” PLoS Biol 20, e3001944. https://doi.org/10.1371/journal.pbio.3001944
Iglesias, N., Currie, M.A., Jih, G., Paulo, J.A., Siuti, N., Kalocsay, M., Gygi, S.P., Moazed, D., 2018. Automethylation-induced conformational switch in Clr4 (Suv39h) maintains epigenetic stability. Nature 560, 504–508. https://doi.org/10.1038/s41586-018-0398-2
Johnsson, A., Durand-Dubief, M., Xue-Franzén, Y., Rönnerblad, M., Ekwall, K., Wright, A., 2009. HAT–HDAC interplay modulates global histone H3K14 acetylation in gene-coding regions during stress. EMBO Reports 10, 1009–1014. https://doi.org/10.1038/embor.2009.127
Kanke, M., Nishimura, K., Kanemaki, M., Kakimoto, T., Takahashi, T.S., Nakagawa, T., Masukata, H., 2011. Auxin-inducible protein depletion system in fission yeast. BMC Cell Biol 12, 8. https://doi.org/10.1186/1471-2121-12-8
Kiani, K., Sanford, E.M., Goyal, Y., Raj, A., 2022. Changes in chromatin accessibility are not concordant with transcriptional changes for single-factor perturbations. Molecular Systems Biology 18, e10979. https://doi.org/10.15252/msb.202210979
Kowalik, K.M., Shimada, Y., Flury, V., Stadler, M.B., Batki, J., Bühler, M., 2015. The Paf1 complex represses small-RNA-mediated epigenetic gene silencing. Nature 520, 248–252. https://doi.org/10.1038/nature14337
Kramer, B.P., Fussenegger, M., 2005. Hysteresis in a synthetic mammalian gene network. Proc. Natl. Acad. Sci. U.S.A. 102, 9517–9522. https://doi.org/10.1073/pnas.0500345102
Kussell, E., Leibler, S., 2005. Phenotypic Diversity, Population Growth, and Information in Fluctuating Environments. Science 309, 2075–2078. https://doi.org/10.1126/science.1114383
Lee, N.N., Chalamcharla, V.R., Reyes-Turcu, F., Mehta, S., Zofall, M., Balachandran, V., Dhakshnamoorthy, J., Taneja, N., Yamanaka, S., Zhou, M., Grewal, S.I.S., 2013. Mtr4-like Protein Coordinates Nuclear RNA Processing for Heterochromatin Assembly and for Telomere Maintenance. Cell 155, 1061–1074. https://doi.org/10.1016/j.cell.2013.10.027
Lenski, R.E., Wiser, M.J., Ribeck, N., Blount, Z.D., Nahum, J.R., Morris, J.J., Zaman, L., Turner, C.B., Wade, B.D., Maddamsetti, R., Burmeister, A.R., Baird, E.J., Bundy, J.,

Grant, N.A., Card, K.J., Rowles, M., Weatherspoon, K., Papoulis, S.E., Sullivan, R., Clark, C., Mulka, J.S., Hajela, N., 2015. Sustained fitness gains and variability in fitness trajectories in the long-term evolution experiment with *Escherichia coli*. Proc. R. Soc. B. 282, 20152292. https://doi.org/10.1098/rspb.2015.2292

Liau, B.B., Sievers, C., Donohue, L.K., Gillespie, S.M., Flavahan, W.A., Miller, T.E., Venteicher, A.S., Hebert, C.H., Carey, C.D., Rodig, S.J., Shareef, S.J., Najm, F.J., van Galen, P., Wakimoto, H., Cahill, D.P., Rich, J.N., Aster, J.C., Suvà, M.L., Patel, A.P., Bernstein, B.E., 2017. Adaptive Chromatin Remodeling Drives Glioblastoma Stem Cell Plasticity and Drug Tolerance. Cell Stem Cell 20, 233-246.e7. https://doi.org/10.1016/j.stem.2016.11.003

Light, W.H., Brickner, D.G., Brand, V.R., Brickner, J.H., 2010. Interaction of a DNA Zip Code with the Nuclear Pore Complex Promotes H2A.Z Incorporation and INO1 Transcriptional Memory. Molecular Cell 40, 112–125. https://doi.org/10.1016/j.molcel.2010.09.007

Luria, S.E., Delbrück, M., 1943. MUTATIONS OF BACTERIA FROM VIRUS SENSITIVITY TO VIRUS RESISTANCE. Genetics 28, 491–511. https://doi.org/10.1093/genetics/28.6.491

McKenzie, G.J., Harris, R.S., Lee, P.L., Rosenberg, S.M., 2000. The SOS response regulates adaptive mutation. Proc. Natl. Acad. Sci. U.S.A. 97, 6646–6651. https://doi.org/10.1073/pnas.120161797

Ogura, M., Wakaiki, M., Preciado, V.M., 2016. Dynamic analysis of bet-hedging strategies as a protection mechanism against environmental fluctuations, in: 2016 IEEE 55th Conference on Decision and Control (CDC). Presented at the 2016 IEEE 55th Conference on Decision and Control (CDC), IEEE, Las Vegas, NV, USA, pp. 4178–4183. https://doi.org/10.1109/CDC.2016.7798903

Park, M., Patel, N., Keung, A.J., Khalil, A.S., 2019. Engineering Epigenetic Regulation Using Synthetic Read-Write Modules. Cell 176, 227-238.e20. https://doi.org/10.1016/j.cell.2018.11.002

Parmentier, R., Racine, L., Moussy, A., Chantalat, S., Sudharshan, R., Papili Gao, N., Stockholm, D., Corre, G., Fourel, G., Deleuze, J.-F., Gunawan, R., Paldi, A., 2022. Global genome decompaction leads to stochastic activation of gene expression as a first step toward fate commitment in human hematopoietic cells. PLoS Biol 20, e3001849. https://doi.org/10.1371/journal.pbio.3001849

Parsa, J.-Y., Boudoukha, S., Burke, J., Homer, C., Madhani, H.D., 2018. Polymerase pausing induced by sequence-specific RNA-binding protein drives heterochromatin assembly. Genes Dev. 32, 953–964. https://doi.org/10.1101/gad.310136.117

Pisacane, P., Halic, M., 2017. Tailing and degradation of Argonaute-bound small RNAs protect the genome from uncontrolled RNAi. Nat Commun 8, 15332. https://doi.org/10.1038/ncomms15332

Ragunathan, K., Jih, G., Moazed, D., 2015. Epigenetic inheritance uncoupled from sequence-specific recruitment. Science 348, 1258699. https://doi.org/10.1126/science.1258699

Raj, A., van Oudenaarden, A., 2008. Nature, Nurture, or Chance: Stochastic Gene Expression and Its Consequences. Cell 135, 216–226. https://doi.org/10.1016/j.cell.2008.09.050

Ravikumar, A., Arzumanyan, G.A., Obadi, M.K.A., Javanpour, A.A., Liu, C.C., 2018. Scalable, Continuous Evolution of Genes at Mutation Rates above Genomic Error Thresholds. Cell 175, 1946-1957.e13. https://doi.org/10.1016/j.cell.2018.10.021

Rubio, A., Ghosh, S., Mülleder, M., Ralser, M., Mata, J., 2021. Ribosome profiling reveals ribosome stalling on tryptophan codons and ribosome queuing upon oxidative stress in fission yeast. Nucleic Acids Research 49, 383–399. https://doi.org/10.1093/nar/gkaa1180

Shaffer, S.M., Dunagin, M.C., Torborg, S.R., Torre, E.A., Emert, B., Krepler, C., Beqiri, M., Sproesser, K., Brafford, P.A., Xiao, M., Eggan, E., Anastopoulos, I.N., Vargas-Garcia, C.A., Singh, A., Nathanson, K.L., Herlyn, M., Raj, A., 2017. Rare cell

variability and drug-induced reprogramming as a mode of cancer drug resistance. Nature 546, 431–435. https://doi.org/10.1038/nature22794
Shaffer, S.M., Emert, B.L., Reyes Hueros, R.A., Cote, C., Harmange, G., Schaff, D.L., Sizemore, A.E., Gupte, R., Torre, E., Singh, A., Bassett, D.S., Raj, A., 2020. Memory Sequencing Reveals Heritable Single-Cell Gene Expression Programs Associated with Distinct Cellular Behaviors. Cell 182, 947-959.e17. https://doi.org/10.1016/j.cell.2020.07.003
Sharma, S.V., Lee, D.Y., Li, B., Quinlan, M.P., Takahashi, F., Maheswaran, S., McDermott, U., Azizian, N., Zou, L., Fischbach, M.A., Wong, K.-K., Brandstetter, K., Wittner, B., Ramaswamy, S., Classon, M., Settleman, J., 2010. A Chromatin-Mediated Reversible Drug-Tolerant State in Cancer Cell Subpopulations. Cell 141, 69–80. https://doi.org/10.1016/j.cell.2010.02.027
Soni, K., Sivadas, A., Horvath, A., Dobrev, N., Hayashi, R., Kiss, L., Simon, B., Wild, K., Sinning, I., Fischer, T., 2023. Mechanistic insights into RNA surveillance by the canonical poly(A) polymerase Pla1 of the MTREC complex. Nat Commun 14, 772. https://doi.org/10.1038/s41467-023-36402-6
Stajic, D., Bank, C., Gordo, I., 2022. Adaptive Potential of Epigenetic Switching During Adaptation to Fluctuating Environments. Genome Biology and Evolution 14, evac065. https://doi.org/10.1093/gbe/evac065
Stajic, D., Perfeito, L., Jansen, L.E.T., 2019. Epigenetic gene silencing alters the mechanisms and rate of evolutionary adaptation. Nat Ecol Evol 3, 491–498. https://doi.org/10.1038/s41559-018-0781-2
Sump, B., Brickner, D.G., D'Urso, A., Kim, S.H., Brickner, J.H., 2022. Mitotically heritable, RNA polymerase II-independent H3K4 dimethylation stimulates INO1 transcriptional memory. eLife 11, e77646. https://doi.org/10.7554/eLife.77646
Tagkopoulos, I., Liu, Y.-C., Tavazoie, S., 2008. Predictive Behavior Within Microbial Genetic Networks. Science 320, 1313–1317. https://doi.org/10.1126/science.1154456
Takahashi, K., Yamanaka, S., 2006. Induction of Pluripotent Stem Cells from Mouse Embryonic and Adult Fibroblast Cultures by Defined Factors. Cell 126, 663–676. https://doi.org/10.1016/j.cell.2006.07.024
Tatarakis, A., Saini, H., Moazed, D., 2023. Requirements for establishment and epigenetic stability of mammalian heterochromatin (preprint). Developmental Biology. https://doi.org/10.1101/2023.02.27.530221
Thattai, M., van Oudenaarden, A., 2004. Stochastic Gene Expression in Fluctuating Environments. Genetics 167, 523–530. https://doi.org/10.1534/genetics.167.1.523
Torres-Garcia, S., Yaseen, I., Shukla, M., Audergon, P.N.C.B., White, S.A., Pidoux, A.L., Allshire, R.C., 2020. Epigenetic gene silencing by heterochromatin primes fungal resistance. Nature 585, 453–458. https://doi.org/10.1038/s41586-020-2706-x
True, H.L., Lindquist, S.L., 2000. A yeast prion provides a mechanism for genetic variation and phenotypic diversity. Nature 407, 477–483. https://doi.org/10.1038/35035005
Wang, J., Reddy, B.D., Jia, S., 2015. Rapid epigenetic adaptation to uncontrolled heterochromatin spreading. eLife 4, e06179. https://doi.org/10.7554/eLife.06179
Wei, Y., Lee, N.N., Pan, L., Dhakshnamoorthy, J., Sun, L.-L., Zofall, M., Wheeler, D., Grewal, S.I.S., 2021. TOR targets an RNA processing network to regulate facultative heterochromatin, developmental gene expression and cell proliferation. Nat Cell Biol 23, 243–256. https://doi.org/10.1038/s41556-021-00631-y
Wong, B.G., Mancuso, C.P., Kiriakov, S., Bashor, C.J., Khalil, A.S., 2018. Precise, automated control of conditions for high-throughput growth of yeast and bacteria with eVOLVER. Nat Biotechnol 36, 614–623. https://doi.org/10.1038/nbt.4151
Yamanaka, S., Mehta, S., Reyes-Turcu, F.E., Zhuang, F., Fuchs, R.T., Rong, Y., Robb, G.B., Grewal, S.I.S., 2013. RNAi triggered by specialized machinery silences developmental genes and retrotransposons. Nature 493, 557–560. https://doi.org/10.1038/nature11716
Yaseen, I., White, S.A., Torres-Garcia, S., Spanos, C., Lafos, M., Gaberdiel, E., Yeboah, R., El Karoui, M., Rappsilber, J., Pidoux, A.L., Allshire, R.C., 2022. Proteasome-

dependent truncation of the negative heterochromatin regulator Epe1 mediates antifungal resistance. Nat Struct Mol Biol 29, 745–758. https://doi.org/10.1038/s41594-022-00801-y

Zhong, Z., Wong, B.G., Ravikumar, A., Arzumanyan, G.A., Khalil, A.S., Liu, C.C., 2020. Automated Continuous Evolution of Proteins *in Vivo*. ACS Synth. Biol. 9, 1270–1276. https://doi.org/10.1021/acssynbio.0c00135

Zofall, M., Sandhu, R., Holla, S., Wheeler, D., Grewal, S.I.S., 2022. Histone deacetylation primes self-propagation of heterochromatin domains to promote epigenetic inheritance. Nat Struct Mol Biol 29, 898–909. https://doi.org/10.1038/s41594-022-00830-7

Zofall, M., Yamanaka, S., Reyes-Turcu, F.E., Zhang, K., Rubin, C., Grewal, S.I.S., 2012. RNA Elimination Machinery Targeting Meiotic mRNAs Promotes Facultative Heterochromatin Formation. Science 335, 96–100. https://doi.org/10.1126/science.1211651

Figure 1: An inducible Epe1 depletion system to trigger heterochromatin misregulation on-demand

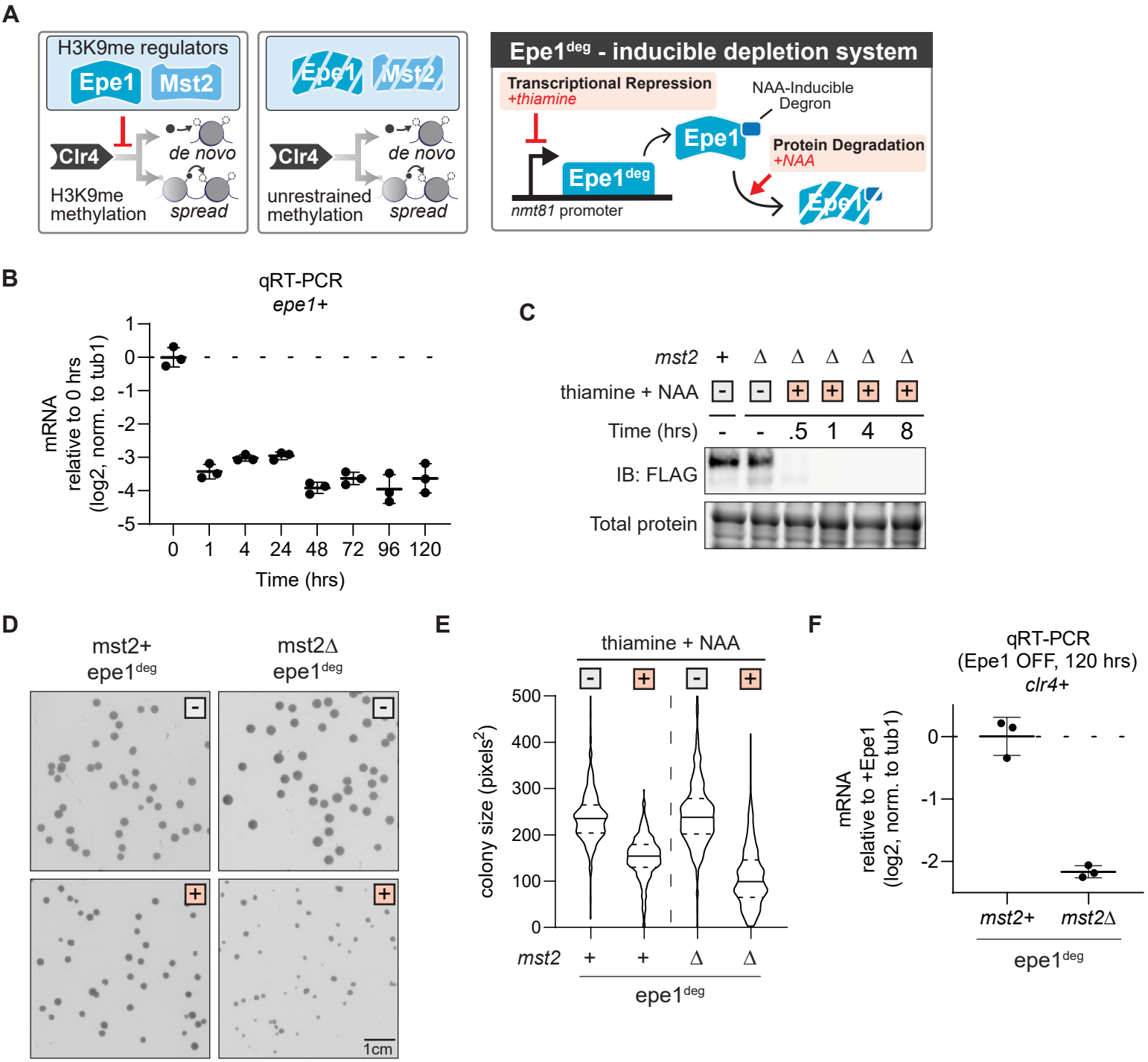

Figure 1. An inducible Epe1 depletion system to trigger heterochromatin misregulation on-demand.

(A) Epe1 and Mst2 regulate H3K9me deposition catalyzed by the H3K9 methyltransferase, Clr4 in *S.pombe.* Epe1 and Mst2 prevent uncontrolled H3K9me spreading. The absence of Mst2 and Epe1 triggers heterochromatin misregulation (Left). Construction of a precision-engineered genetic approach to toggle Epe1 availability in cells ($Epe1^{deg}$). Epe1 transcription is regulated by a thiamine inducible nmt81 promoter and protein levels are regulated by an auxin-inducible degron tag (AID). Adding auxin and thiamine promotes the on-demand, inducible depletion of Epe1 (Right).

(B) *epe1+* mRNA expression measured by qRT-PCR as a function of time following treatment with 15μM thiamine and 0.5mM NAA. Log2 fold-change of mRNA is measured relative to cells without thiamine and NAA (0 hrs). Error bars represent standard deviation, N=3.

(C) Western blot for Epe1-3xFLAG-AID in $Epe1^{deg}$ strains. Media type is indicated with either a white box for no treatment, or an orange box for media with 15μM thiamine and 0.5mM NAA. Total protein levels are shown in the lower panel.

(D) Examples of *S.pombe* colonies on solid media after three days of growth. Media type is indicated with either a white box for no treatment, or an orange box for media with 15μM thiamine and 0.5mM NAA. Image colors are inverted to highlight cell colonies.

(E) Colony size distribution measured as pixel area in different genetic backgrounds and growth conditions. Cell size quantified after five days of growth. Media type is indicated with either a white box for no treatment, or an orange box for media with 15μM thiamine and 0.5mM NAA. Mean and st. dev of distributions in $pixels^2$: *mst2+* $epe1^{deg}$ no treatment (240.4 ± 64.2), thiamine and NAA (151.2 ± 46.6); *mst2*Δ $epe1^{deg}$ no treatment (246.2 ± 74.6), thiamine and NAA (109.4 ± 64.0)

(F) *clr4+* mRNA expression measured by qRT-PCR after five days of treatment with 15μM thiamine and 0.5mM NAA. Log2 fold-change expression of mRNA is relative to mRNA expression without thiamine and NAA. Error bars represent standard deviation, N=3.

Figure 2: Time evolution of adaptive silencing during heterochromatin misregulation

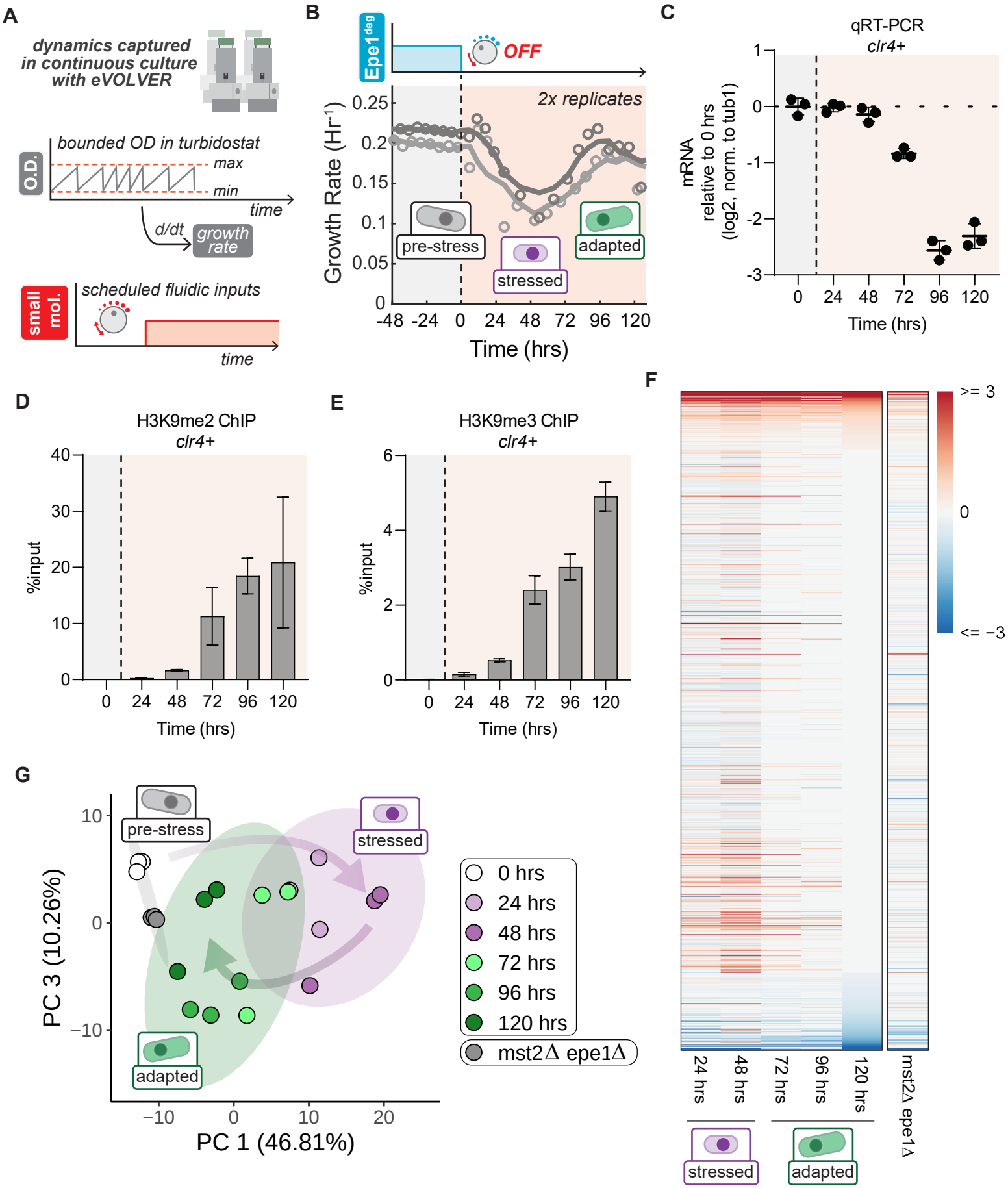

Figure 2. Time evolution of adaptive silencing during heterochromatin misregulation.

(A) Model of the eVOLVER continuous culture system used to control growth of *mst2*Δ *epe1*^{deg} cells using a continuous turbidostat routine, with real-time quantification of growth rate and the ability to schedule media changes.

(B) Real-time monitoring of growth rates of *mst2*Δ *epe1*^{deg} in eVOLVER. Treatment with 15μM thiamine and 0.5mM NAA was initiated at t=0hrs. Individual trendlines indicate replicates (N=2). Orange shaded portion represents the time period during which Epe1 has been depleted.

(C) *clr4*+ mRNA expression measured by qRT-PCR as a function of time following treatment with 15μM thiamine and 0.5mM NAA. Log2 fold-change of mRNA is measured relative to cells without thiamine and NAA (0 hrs). Orange shaded portion represents the time period during which Epe1 has been depleted. Error bars represent standard deviation, N=3.

(D) H3K9me2 ChIP-qPCR measured at the *clr4*+ locus as a function of time following treatment with 15μM thiamine and 0.5mM NAA. The orange shaded portion represents the time period during which Epe1 has been depleted. Error bars represent standard deviation, N=2.

(E) H3K9me3 ChIP-qPCR measured at the *clr4*+ locus as a function of time following treatment with 15μM thiamine and 0.5mM NAA. Orange shaded portion represents the time period during which Epe1 has been depleted. Error bars represent standard deviation, N=2.

(F) Heatmap of significant differentially expressed genes following treatment with thiamine and auxin relative to untreated *mst2*Δ *epe1*^{deg} cells. Heatmap consists of genes that are differentially expressed at least during one time point. Total number of differentially expressed transcripts N=3896, significance cutoff of AdjPval ≤ 0.01.

(G) Time course PCA analysis of the regularized log transform of RNAseq normalized counts denoting different time points after treatment with15μM thiamine and 0.5mM NAA. Colors denote pre-stress, stress and adapted cell phases. N=3, ellipse level=0.9.

Figure 3: Heterochromatin misregulation triggers the targeted expansion of pre-existing H3K9me3 islands and leads to the silencing of a small fraction of essential genes.

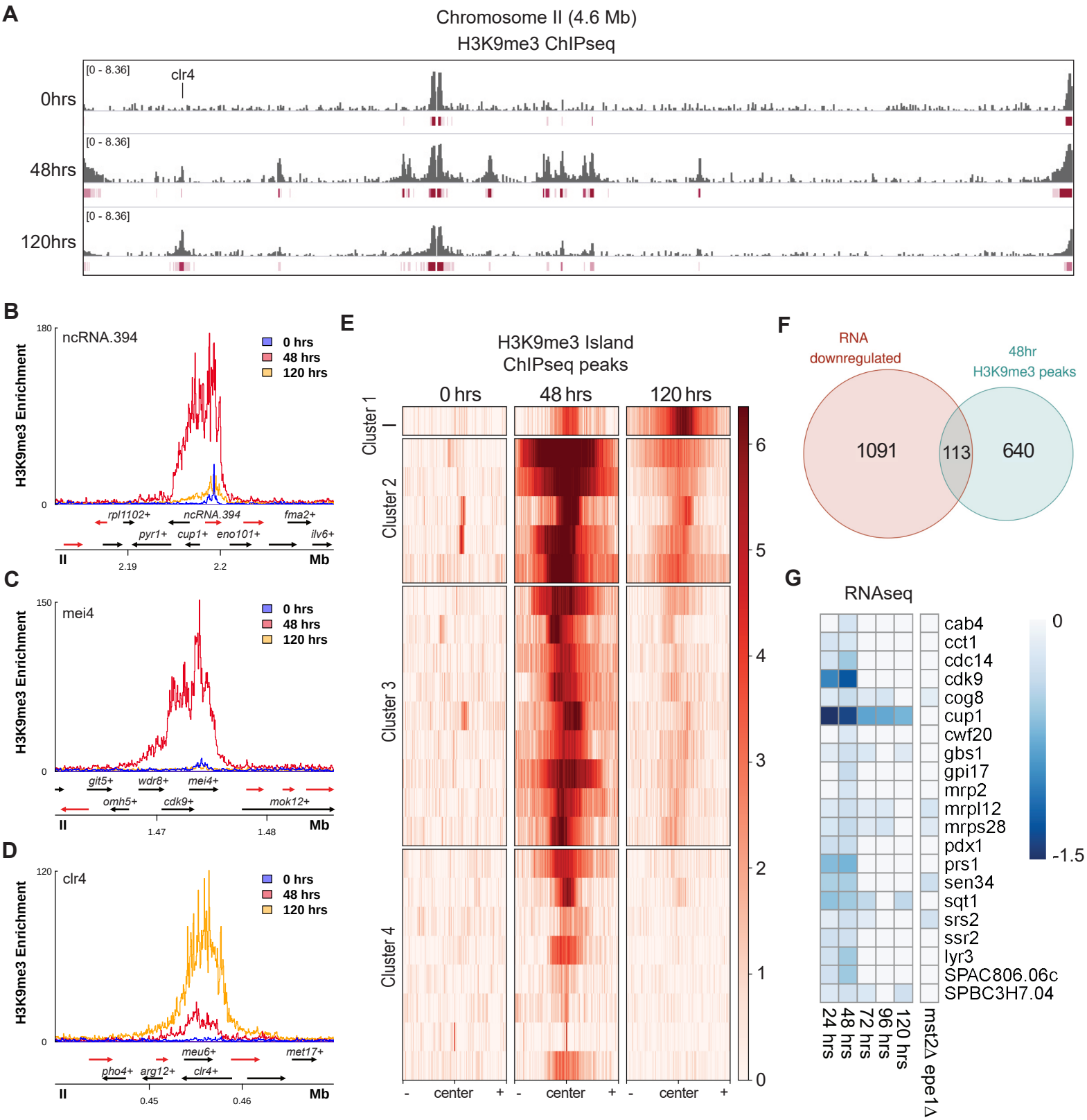

Figure 3. Heterochromatin misregulation triggers the targeted expansion of pre-existing H3K9me3 islands

(A) H3K9me3 ChIP-seq tracks of chromosome II of the *S. pombe* genome. Enrichment is shown in log2 fold change of IP normalized to input. Time of Epe1 depletion is indicated on the left side of each track. Peaks identified are denoted in red below each track. The *clr4+* gene locus is specifically highlighted. One of two ChIP-seq replicates is shown in this figure.

(B) H3K9me3 ChIP-seq enrichment centered on *ncRNA.394* for the indicated time points. Genomic tracks below show coding transcripts in black, non-coding transcripts in red.

(C) H3K9me3 ChIP-seq enrichment centered on *mei4+* for the indicated time points. Genomic tracks below show coding transcripts in black, non-coding transcripts in red.

(D) H3K9me3 ChIP-seq enrichment centered on *clr4+* for the indicated time points. Genomic tracks below show coding transcripts in black, non-coding transcripts in red.

(E) Heatmap with k-means clustered H3K9me3 islands during heterochromatin misregulation at 0hrs, 48hrs, and 120hrs of Epe1 depletion in *mst2*Δ *epe1*^{deg}.

(F) Venn diagram depicting genes that are downregulated (AdjPval ≤ 0.01) by 48 hours after Epe1 depletion, overlapped with genes marked by H3K9me3 selectively at 48 hours.

(G) Heatmap depicting the expression dynamics of essential genes selectively marked by H3K9me3 at 48 hours. Changes in expression are log2 fold change relative to untreated *mst2*Δ *epe1*^{deg} cells. (AdjPval ≤ 0.01)

Figure 4: Activation of the cellular stress response pathway is required for survival but not adaptive choice

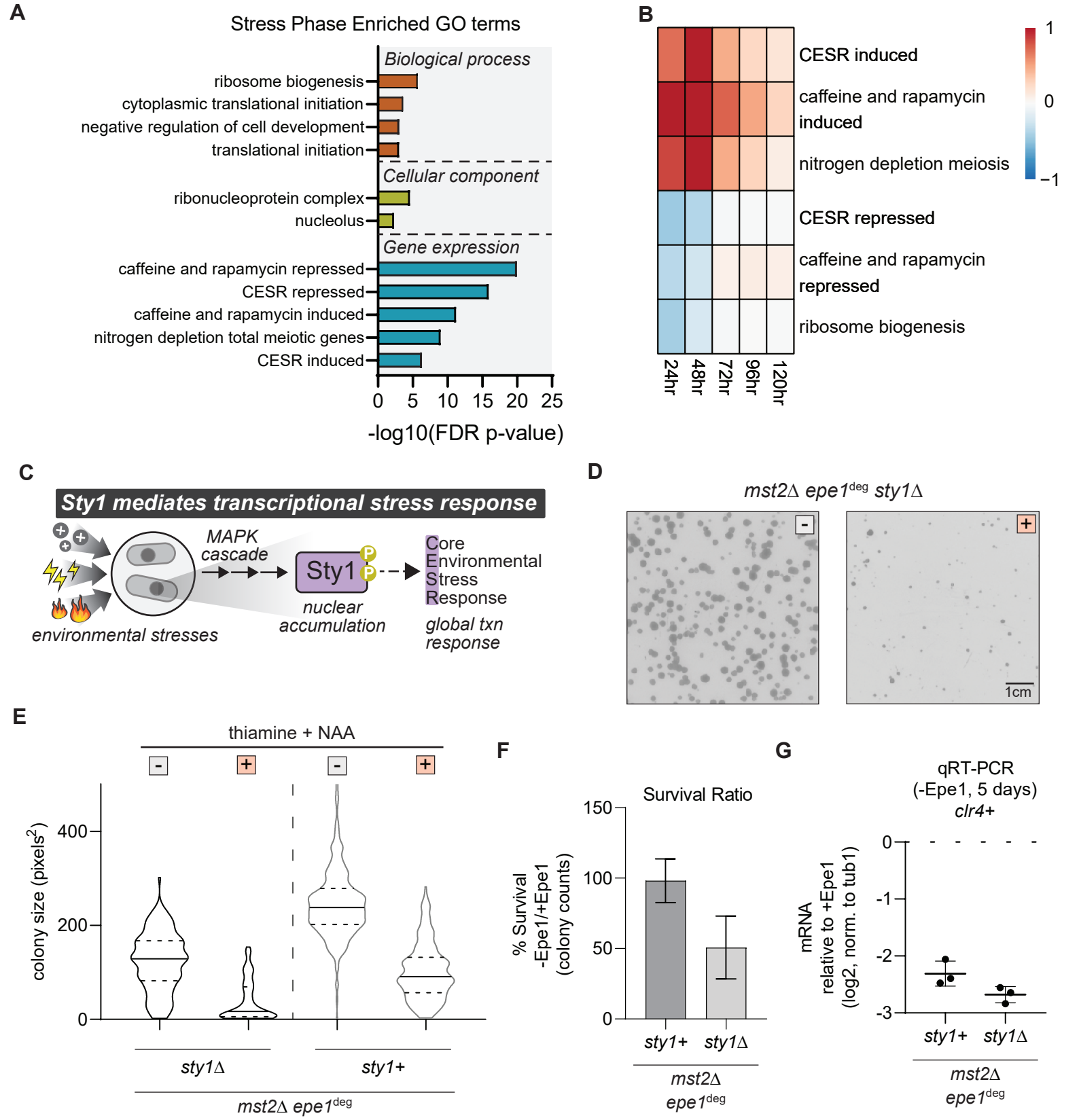

Figure 4 Activation of the cellular stress response pathway is required for survival but not adaptive choice

(A) Selected GO terms for genes differentially expressed (AdjPval ≤ 0.01) within stress phase (48 hours of Epe1 depletion). GO significance cutoff was set as FDR p-value ≤ 0.01.
(B) Heatmap showing average fold change for genes differentially expressed (AdjPval ≤ 0.01) in selected GO categories, relative to untreated *mst2*Δ *epe1*^{deg} cells.
(C) Environmental stresses trigger a stress-activated MAPK cascade that phosphorylates Sty1, which drives a global transcriptional response that includes the core environmental stress response.
(D) Examples of *mst2*Δ *epe1*^{deg} *sty1*Δ *S.pombe* colonies on solid media after three days of growth. Media type is indicated with either a white box for no treatment, or an orange box for media with 15μM thiamine and 0.5mM NAA. Image colors are inverted to highlight cell colonies.
(G) Colony size distribution, in pixel area, under different growth conditions. Cell size quantified after five days of growth. Genotype and media treatment is indicated on the x-axis. Media type is indicated with either a white box for no treatment, or an orange box for media with 15μM thiamine and 0.5mM NAA. Mean and st. dev of distributions in pixels^2: *mst2*Δ *epe1*^{deg} *sty1*Δ no treatment (123.0 ± 61.9), thiamine and NAA (39.1 ± 43.2); *mst2*Δ *epe1*^{deg} no treatment (246.2 ± 74.6), thiamine and NAA (109.4 ± 64.0)
(E) Percentage of *mst2*Δ *epe1*^{deg} *sty1+* and *mst2*Δ *epe1*^{deg} *sty1*Δ cells that survive following treatment with 15μM thiamine and 0.5mM NAA. Total colony count ratios were calculated by total number of colonies with thiamine and NAA divided by total number of colonies grown without thiamine and NAA.
(F) *clr4+* mRNA expression measured by qRT-PCR in *mst2*Δ *epe1*^{deg} *sty1+* and *mst2*Δ *epe1*^{deg} *sty1*Δ after five days of treatment with 15μM thiamine and 0.5mM NAA. Log2 fold-change expression of mRNA is relative to expression without thiamine and NAA.

Figure 5: Adaptive heterochromatin exhibits memory upon re-induction of stress

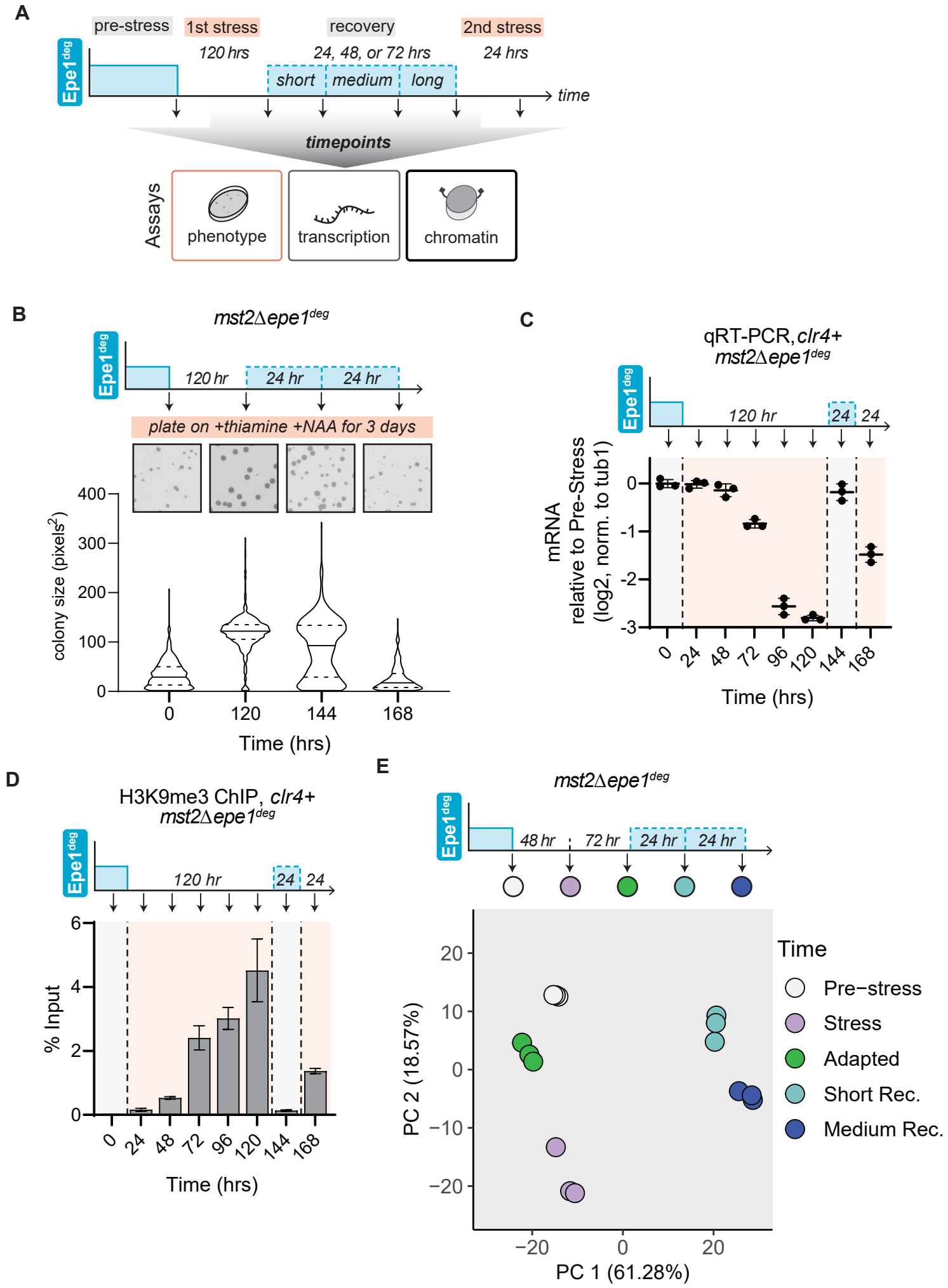

Figure 5. Adaptive heterochromatin exhibits memory upon re-induction of stress.

(A) Schematic indicating cycling of Epe1 availability in *mst2*Δ *epe1*^{deg} to measure epigenetic memory at the phenotype, transcription and chromatin level. Pre-stress cells express Epe1 and have not experienced heterochromatin misregulation. Adapted cells have experienced Epe1 depletion and silenced *clr4+* after 120 hours. Cells were allowed to recover with Epe1 expressed for 24, 48 or 72 hours, followed by a second round of Epe1 depletion.

(B) Colony size distribution of *mst2*Δ *epe1*^{deg} cells, in pixel area, after three days of growth with Epe1 depletion from 15μM thiamine and 0.5mM NAA (Bottom). Epe1 expression and snapshots of culture plates (Top). Mean and st. dev of distributions in pixels^2: 0 hours (34.5 ± 27.3), 120 hours (118.9 ± 37.6), 144 hours (87.3 ± 59.4), 168 hours (26.3 ± 25.9)

(C) mRNA expression in *mst2*Δ *epe1*^{deg} cells measured by qRT-PCR for *clr4+*. Orange shaded portion represents the time period during which Epe1 has been depleted. Epe1 expression and time points are shown above the figure.

(D) H3K9me3 ChIP-qPCR measuring enrichment at the *clr4+* locus. Orange shaded portion represents the time period during which Epe1 has been depleted. Epe1 expression and time points are shown above the figure. N=2 replicates.

(E) Time course PCA analysis of the regularized log transform of RNAseq normalized counts denoting different time points after treatment with15μM thiamine and 0.5mM NAA. Colors denote pre-stress, stress, adapted, and recovery cell phases. N=3, ellipse level=0.9. Epe1 expression and time points are shown above the figure.

Figure 6: The time scale of adaptive memory can be tuned by histone acetylation

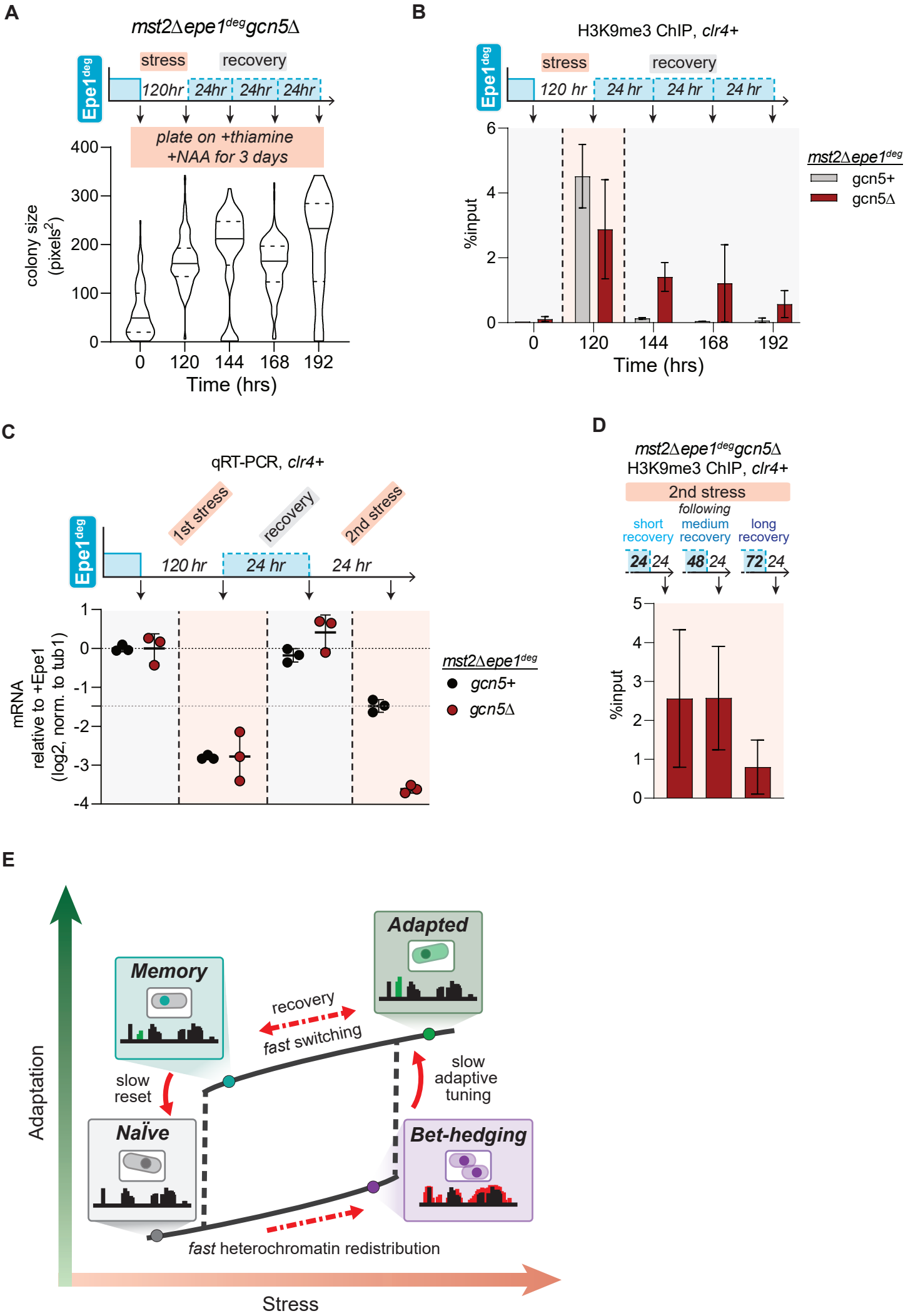

Figure 6 The time scale of adaptive memory can tuned by histone acetylation.

(A) Colony size distribution of *mst2*Δ *epe1*^{deg} *gcn5*Δ cells, in pixel area, after three days of growth with Epe1 depletion from 15μM thiamine and 0.5mM NAA. Mean and st. dev of distributions in pixels^2: 0 hours (61.9 ± 53.8), 120 hours (166.1 ± 50.9), 144 hours (185.8 ± 87.9), 168 hours (158.2 ± 54.0), 192 hours (201.1 ± 102.3)

(B) H3K9me3 ChIP-qPCR measuring enrichment at the *clr4*+ locus. Orange shaded portion represents the time period during which Epe1 has been depleted. Epe1 expression and time points are shown above the figure. N=2 replicates.

(C) *clr4*+ mRNA expression in in *mst2*Δ *epe1*^{deg} *gcn5*+ and *mst2*Δ *epe1*^{deg} *gcn5*Δ cells measured by qRT-PCR. Orange shaded portion represents the time period during which Epe1 has been depleted.

(D) H3K9me3 ChIP-qPCR measuring enrichment at the *clr4*+ locus in *mst2*Δ *epe1*^{deg} *gcn5*Δ cells. Orange shaded portion represents the time period during which Epe1 has been depleted. N=2 replicates.

(E) Heterochromatin-defining H3K9 methylation (H3K9me), normally reserved to maintain genome integrity can be redistributed across the genome to establish new and potentially adaptive phenotypes. Establishing adaptive H3K9me patterns occurs over surprisingly slow time-scales relative to the initiating stress. The slow kinetics of adaptation may serve as a bet-hedging strategy for cells to decipher optimal survival solutions. Upon removal of stress, cells relax to new transcriptional and chromatin states rather than revert to their initial (ground) state, establishing a tunable memory for a future adaptive epigenetic response. Cells exhibit history dependence wherein a prior exposure to stress locks cells in a new transcriptional state that encodes adaptive memory.